

RESEARCH ARTICLE

10.1029/2017JD027978

Key Points:

- Based on winter 2014 observations, very short-lived bromocarbons produced by oceanic biology contribute  $5 \pm 2$  ppt to stratospheric bromine
- Of the bromine from very short-lived substances that reaches the stratosphere, 60% enters as organic species and 40% as inorganic species
- Representation of stratospheric bromine within global models is greatly improved upon consideration of very short-lived bromocarbons

Supporting Information:

- Supporting Information S1

Correspondence to:

P. A. Wales,  
pwales@umd.edu

Citation:

Wales, P. A., Salawitch, R. J., Nicely, J. M., Anderson, D. C., Canty, T. P., Baidar, S., et al. (2018). Stratospheric injection of brominated very short-lived substances: Aircraft observations in the Western Pacific and representation in global models. *Journal of Geophysical Research: Atmospheres*, 123. <https://doi.org/10.1029/2017JD027978>

Received 27 OCT 2017

Accepted 1 MAY 2018

Accepted article online 14 MAY 2018

## Stratospheric Injection of Brominated Very Short-Lived Substances: Aircraft Observations in the Western Pacific and Representation in Global Models

Pamela A. Wales<sup>1</sup> , Ross J. Salawitch<sup>1,2,3</sup> , Julie M. Nicely<sup>1,4,5</sup> , Daniel C. Anderson<sup>2,6</sup> , Timothy P. Canty<sup>2</sup> , Sunil Baidar<sup>7,8,9,10</sup> , Barbara Dix<sup>7</sup> , Theodore K. Koenig<sup>7,8</sup> , Rainer Volkamer<sup>7,8</sup> , Dexian Chen<sup>11</sup> , L. Gregory Huey<sup>11</sup> , David J. Tanner<sup>11</sup> , Carlos A. Cuevas<sup>12</sup> , Rafael P. Fernandez<sup>12,13</sup> , Douglas E. Kinnison<sup>14</sup> , Jean-Francois Lamarque<sup>14</sup> , Alfonso Saiz-Lopez<sup>12</sup> , Elliot L. Atlas<sup>15</sup> , Samuel R. Hall<sup>14</sup> , Maria A. Navarro<sup>15</sup> , Laura L. Pan<sup>14</sup> , Sue M. Schauffler<sup>14</sup> , Meghan Stell<sup>14,16</sup> , Simone Tilmes<sup>14</sup> , Kirk Ullmann<sup>14</sup> , Andrew J. Weinheimer<sup>14</sup> , Hideharu Akiyoshi<sup>17</sup> , Martyn P. Chipperfield<sup>18</sup> , Makoto Deushi<sup>19</sup> , Sandip S. Dhomse<sup>18</sup> , Wuhu Feng<sup>18</sup> , Phoebe Graf<sup>20</sup> , Ryan Hossaini<sup>21</sup> , Patrick Jöckel<sup>20</sup> , Eva Mancini<sup>22</sup> , Martine Michou<sup>23</sup> , Olaf Morgenstern<sup>24</sup> , Luke D. Oman<sup>4</sup> , Giovanni Pitari<sup>25</sup> , David A. Plummer<sup>26</sup> , Laura E. Revell<sup>27,28</sup> , Eugene Rozanov<sup>27,29</sup> , David Saint-Martin<sup>23</sup> , Robyn Schofield<sup>30,31</sup> , Andrea Stenke<sup>27</sup> , Kane A. Stone<sup>30,31,32</sup> , Daniele Visoni<sup>22</sup> , Yousuke Yamashita<sup>17,33</sup> , and Guang Zeng<sup>24</sup> 

<sup>1</sup>Department of Chemistry and Biochemistry, University of Maryland, College Park, MD, USA, <sup>2</sup>Department of Atmospheric and Oceanic Science, University of Maryland, College Park, MD, USA, <sup>3</sup>Earth System Science Interdisciplinary Center, University of Maryland, College Park, MD, USA, <sup>4</sup>Atmospheric Chemistry and Dynamics Laboratory, NASA Goddard Space Flight Center, Greenbelt, MD, USA, <sup>5</sup>Universities Space Research Association, Columbia, MD, USA, <sup>6</sup>Now at Department of Chemistry, Drexel University, Philadelphia, PA, USA, <sup>7</sup>Department of Chemistry and Biochemistry, University of Colorado Boulder, Boulder, CO, USA, <sup>8</sup>Cooperative Institute for Research in Environmental Sciences, Boulder, CO, USA, <sup>9</sup>National Oceanic and Atmospheric Administration, Boulder, CO, USA, <sup>10</sup>Now at NOAA Earth System Research Laboratory Chemical Sciences Division, Boulder, CO, USA, <sup>11</sup>School of Earth and Atmospheric Sciences, Georgia Tech, Atlanta, GA, USA, <sup>12</sup>Department of Atmospheric Chemistry and Climate, Institute of Physical Chemistry Rocasolano, Spanish National Research Council (CSIC), Madrid, Spain, <sup>13</sup>Argentine National Research Council (CONICET), FCEN-UNCuyo, UTN-FRM, Mendoza, Argentina, <sup>14</sup>National Center for Atmospheric Research, Boulder, CO, USA, <sup>15</sup>Department of Atmospheric Sciences, Rosenstiel School of Marine and Atmospheric Science, University of Miami, Miami, FL, USA, <sup>16</sup>Now at Undergraduate Research Opportunities Center, California State University, Monterey Bay, Seaside, CA, USA, <sup>17</sup>National Institute for Environmental Studies, Tsukuba, Japan, <sup>18</sup>School of Earth and Environment, University of Leeds, Leeds, UK, <sup>19</sup>Meteorological Research Institute, Tsukuba, Japan, <sup>20</sup>Deutsches Zentrum für Luft- und Raumfahrt, Institut für Physik der Atmosphäre, Oberpfaffenhofen, Germany, <sup>21</sup>Lancaster Environment Centre, Lancaster University, Lancaster, UK, <sup>22</sup>Department of Physical and Chemical Sciences and Center of Excellence CETEMPS, Università dell'Aquila, L'Aquila, Italy, <sup>23</sup>CNRM UMR 3589, Météo-France/CNRS, Toulouse, France, <sup>24</sup>National Institute of Water and Atmospheric Research, Wellington, New Zealand, <sup>25</sup>Department of Physical and Chemical Sciences, Università dell'Aquila, L'Aquila, Italy, <sup>26</sup>Environment and Climate Change Canada, Montréal, Quebec, Canada, <sup>27</sup>Institute for Atmospheric and Climate Science, ETH Zürich, Zürich, Switzerland, <sup>28</sup>Bodeker Scientific, Christchurch, New Zealand, <sup>29</sup>Physikalisch-Meteorologisches Observatorium Davos, World Radiation Centre, Davos Dorf, Switzerland, <sup>30</sup>School of Earth Sciences, University of Melbourne, Melbourne, Victoria, Australia, <sup>31</sup>ARC Centre of Excellence for Climate System Science, Sydney, New South Wales, Australia, <sup>32</sup>Now at Massachusetts Institute of Technology, Boston, MA, USA, <sup>33</sup>Now at Japan Agency for Marine-Earth Science and Technology, Yokohama, Japan

**Abstract** We quantify the stratospheric injection of brominated very short-lived substances (VLSs) based on aircraft observations acquired in winter 2014 above the Tropical Western Pacific during the CONvective TRansport of Active Species in the Tropics (CONTRAST) and the Airborne Tropical Tropopause EXperiment (ATTREX) campaigns. The overall contribution of VLSs to stratospheric bromine was determined to be  $5.0 \pm 2.1$  ppt, in agreement with the  $5 \pm 3$  ppt estimate provided in the 2014 World Meteorological Organization (WMO) Ozone Assessment report (WMO 2014), but with lower uncertainty. Measurements of organic bromine compounds, including VLSs, were analyzed using CFC-11 as a reference stratospheric tracer. From this analysis,  $2.9 \pm 0.6$  ppt of bromine enters the stratosphere via organic source gas injection of VLSs. This value is two times the mean bromine content of VLSs measured at the tropical tropopause, for regions outside of the Tropical Western Pacific, summarized in WMO 2014. A photochemical box model,

constrained to CONTRAST observations, was used to estimate inorganic bromine from measurements of BrO collected by two instruments. The analysis indicates that  $2.1 \pm 2.1$  ppt of bromine enters the stratosphere via inorganic product gas injection. We also examine the representation of brominated VSLS within 14 global models that participated in the Chemistry-Climate Model Initiative. The representation of stratospheric bromine in these models generally lies within the range of our empirical estimate. Models that include explicit representations of VSLS compare better with bromine observations in the lower stratosphere than models that utilize longer-lived chemicals as a surrogate for VSLS.

## 1. Introduction

Bromine chemistry plays an important role in the depletion of stratospheric ozone (Wofsy et al., 1975). Historically, the only sources of stratospheric bromine considered in many model calculations of ozone depletion and recovery had been methyl bromide ( $\text{CH}_3\text{Br}$ ) and halons (e.g., Douglass et al., 2011). However, numerous studies have indicated that marine biogenic emissions of brominated very short-lived substances (VSLS) constitute an important source of stratospheric bromine (Dorf et al., 2008; Dvortsov et al., 1999; Ko et al., 1997; Pfeilsticker et al., 2000; Salawitch et al., 2005). It has been shown that incorporating VSLS into models improves agreement between simulated and measured trends in column ozone (Feng et al., 2007; Salawitch et al., 2005; Sinnhuber & Meul, 2015) and has a significant effect on projections of the depth and potentially the timing for the recovery of the Antarctic ozone hole (Fernandez et al., 2017; Oman et al., 2016). Additionally, the inclusion of VSLS alters the modeled sensitivity of the ozone layer to both future volcanic eruptions (Klobas et al., 2017) and geoengineering of climate via injection of stratospheric sulfate (Tilmes et al., 2012, 2008). Finally, accurate calculations of tropospheric bromine monoxide (BrO) loading based on satellite measurements of total column BrO rely on proper representation of the stratospheric injection of brominated VSLS (Choi et al., 2012; Salawitch et al., 2010; Theys et al., 2011).

VSLS are compounds that have lifetimes of six months or less due to photochemical loss in the global troposphere. Since compounds with lifetimes less than six months cannot be assumed to be well mixed within the troposphere (Ko et al., 2003), the stratospheric input of VSLS is more sensitive to the geographic location of their atmospheric sources than the input of  $\text{CH}_3\text{Br}$  and halons, which have atmospheric lifetimes ranging from 0.8 to 65 years. Thus, emissions of VSLS in regions of active, vigorous convection (such as the Tropical Western Pacific, TWP) have a much larger probability of reaching the tropical tropopause layer (TTL) without being chemically altered than compounds released in other areas (e.g., Aschmann et al., 2009; Fernandez et al., 2014; Hossaini et al., 2013).

Here we use the abbreviation VSLS to refer solely to brominated VSLS. The VSLS relevant to this study (i.e.,  $\text{CHBr}_3$ ,  $\text{CH}_2\text{Br}_2$ ,  $\text{CH}_2\text{BrCl}$ ,  $\text{CHBr}_2\text{Cl}$ , and  $\text{CHBrCl}_2$ ) are produced by phytoplankton or algae in the upper ocean (e.g., Carpenter & Liss, 2000; Quack & Wallace, 2003; Tokarczyk & Moore, 1994). The bromine contained in VSLS can reach the stratosphere either via source gas injection (SGI) or product gas injection (PGI). If the VSLS reach the stratosphere in the original organic form (termed  $\text{CBr}_y$ ), this is considered SGI. Alternatively, if the VSLS are oxidized in the troposphere, the constituent bromine atoms rapidly produce inorganic bromine compounds (termed  $\text{Br}_y$ ) such as BrO, Br, HBr, HOBr,  $\text{BrONO}_2$ ,  $\text{BrNO}_2$ ,  $\text{Br}_2$ , and BrCl. If the tropospheric  $\text{Br}_y$  product gases reach the stratosphere, this is termed PGI. Consequently, SGI and PGI are sensitive to the strength of convection relative to the lifetime of the VSLS as well as the partitioning of product gases into soluble compounds that are susceptible to both washout and heterogeneous recycling (Aschmann et al., 2011; Fernandez et al., 2014; Hossaini et al., 2010; Liang et al., 2014, 2010; Schofield et al., 2011; Sinnhuber & Folkins, 2006; Tegtmeier et al., 2012).

Prior estimates of the contribution of VSLS to the stratospheric bromine loading are summarized in the most recent World Meteorological Organization (WMO) Ozone Assessment (WMO 2014; Carpenter et al., 2014). The total contribution of VSLS to stratospheric bromine (i.e., SGI + PGI, denoted  $\text{Br}_y^{\text{VSLS}}$ ) was assessed to be  $5 \pm 3$  parts per trillion by volume (ppt). The best estimate for SGI of VSLS ( $\text{SGI}^{\text{VSLS}}$ ) presented in WMO 2014 is 1.4 ppt, with a range of 0.7 to 3.4 ppt, based on measurements of VSLS at the average tropical tropopause height of 17 km (e.g., Brinckmann et al., 2012; Laube et al., 2008; Schauffler et al., 1999). Observations of  $\text{Br}_y$  compounds at the tropical tropopause are sparse (Dorf et al., 2008; Werner et al., 2017). As a result, PGI has previously been estimated to be 1.1 to 4.3 ppt based on a range of global model simulations

considering the chemical processing of VSLs released by oceanic emissions (Aschmann & Sinnhuber, 2013; Hossaini et al., 2012; Liang et al., 2014, 2010). The WMO 2014 estimate for PGI is consistent with the abundance of  $\text{Br}_y$  reported around 17 km in the tropics by Dorf et al. (2008) as well as the range of  $\text{Br}_y$  mixing ratios at the base of the TTL and above the cold point tropopause reported by Werner et al. (2017). The combined observed  $\text{SGI}^{\text{VSLs}}$  and modeled PGI value generally agrees with estimates of  $\text{Br}_y^{\text{VSLs}}$  that are based on analysis of slant column measurements of BrO in the middle to upper stratosphere (e.g., Dorf et al., 2008; Parrella et al., 2013; Schofield et al., 2004). However, there are significant uncertainties concerning the modeled estimates of PGI (e.g., Liang et al., 2014; Sinnhuber & Folkins, 2006; Tegtmeier et al., 2012) as well as the inference of  $\text{Br}_y$  from measurements of BrO for photochemically aged stratospheric air (Kreycky et al., 2013; Sioris et al., 2006).

In this study we use measurements of organic source gases and BrO, collected in the TTL and lower stratosphere of the TWP, to quantify both  $\text{SGI}^{\text{VSLs}}$  and PGI. The TWP, particularly during boreal winter, is a region of active convection and one of the most important pathways for compounds with short tropospheric lifetimes to reach the stratosphere (Aschmann et al., 2009; Bergman et al., 2012; Levine et al., 2007; Schofield et al., 2011). Consequently, the TWP and nearby Southeast Asia have been regions where a number of ground and ship-based campaigns have been conducted to study oceanic emissions of VSLs (Brinckmann et al., 2012; Mohd Nadzir et al., 2014; Robinson et al., 2014). Additionally, aircraft campaigns observed mixing ratios of VSLs in Southeast Asia that were slightly elevated with respect to measurements collected in the rest of the tropics (Sala et al., 2014; Wisher et al., 2014). However, past campaigns in the TWP did not sample the TTL or the lower stratosphere. Strong convection and potentially suppressed mixing ratios of OH (Rex et al., 2014) could enable efficient transport of VSLs to the TTL. Due to uncertainties in the removal of product gases (Liang et al., 2014; Sinnhuber & Folkins, 2006; Tegtmeier et al., 2012) as well as the transport of source gases within the TTL, direct observations of VSLs and their product gases within air entering the stratosphere are required to better constrain  $\text{SGI}^{\text{VSLs}}$  and PGI.

In the winter of 2014, three aircraft campaigns based in Guam (13.5°N, 144.8°E) extensively sampled the TWP at different heights, including the TTL and lower stratosphere. Our study is based on analysis of data collected during the National Aeronautics and Space Administration (NASA) Airborne Tropical Tropopause Experiment (ATTREX; Jensen et al., 2017) and the National Science Foundation (NSF) Convective Transport of Active Species in the Tropics (CONTRAST; Pan et al., 2017) campaigns. The ATTREX campaign sampled air masses up to 20 km, while CONTRAST included measurements up to 15 km. A third campaign, Coordinated Airborne Studies in the Tropics (CAST; Harris et al., 2017), provided measurements of VSLs (Andrews et al., 2016) and BrO (Le Breton et al., 2017) from the marine boundary layer up to 8 km over the TWP. Since our emphasis is on analysis of observations within and above the TTL, including the lower stratosphere, data from CAST are not shown.

We rely on measurements of  $\text{CH}_3\text{Br}$ , halons, and a suite of organic VSLs provided by the Whole Air Sampler (WAS) instruments (Navarro et al., 2015) during both ATTREX and CONTRAST. We also utilize measurements of BrO obtained by two instruments during CONTRAST: in situ observations from a Chemical Ionization Mass Spectrometer (CIMS; Chen et al., 2016) and remote observations from an Airborne Multi AXis Differential Optical Absorption Spectroscopy (AMAX-DOAS) instrument (Koenig et al., 2017). A limb-scanning mini-Differential Optical Absorption Spectroscopy (mini-DOAS) instrument measured BrO during ATTREX (Stutz et al., 2017; Werner et al., 2017). However, at the time of writing, observations of BrO from the mini-DOAS for the winter 2014 phase of ATTREX are not available.

Our study builds upon prior analyses of ATTREX and CONTRAST data. Navarro et al. (2015) presented an estimate of  $\text{SGI}^{\text{VSLs}}$  based on WAS observations of  $\text{CBr}_y$  compounds acquired during ATTREX and PGI based solely on a model estimate of gas phase  $\text{Br}_y$ . Both Chen et al. (2016) and Koenig et al. (2017) estimated PGI using observations of BrO at the base of the stratosphere acquired during CONTRAST but did not incorporate measurements of  $\text{CBr}_y$ . In this study, we use empirical bromocarbon-tracer relations to combine all three sets of measurements (i.e., WAS organics plus CIMS and AMAX-DOAS BrO) to develop comprehensive, observation-based estimates of  $\text{SGI}^{\text{VSLs}}$ , PGI, and overall  $\text{Br}_y^{\text{VSLs}}$ . Since our study examines measurements obtained within the lower stratosphere and includes a method for quantifying the contribution to BrO from the stratospheric decomposition of  $\text{CBr}_y$  source gases, our value of PGI is likely more robust than prior estimates because a larger ensemble of air masses is represented. We have made no attempt to quantify the amount of PGI that results from the oxidation of VSLs versus other sources, such as sea-salt aerosol. We refer the interested reader to Koenig et al. (2017) for analysis concerning the possible contributions of sea-salt aerosol as well as stratospheric injection of brominated particles to PGI.

We also compare the combined CONTRAST and ATTREX based estimate of  $\text{Br}_y^{\text{VLS}}$  to the equivalent representation of this contribution within 14 global models that participated in the Chemistry-Climate Model Initiative (CCMI; Morgenstern et al., 2017). These global models simulate factors that govern tropospheric chemistry, climate change, and ozone depletion. Eyring et al. (2013) recommended that CCMI models incorporate the WMO 2011 best estimate for  $\text{Br}_y^{\text{VLS}}$  of 5 ppt (Montzka et al., 2011) in one of two manners: either by explicitly including  $\text{CHBr}_3$  and  $\text{CH}_2\text{Br}_2$  (the two major VLS) in the model or by increasing the surface mixing ratio of  $\text{CH}_3\text{Br}$  (a traditional, non-VLS source of bromine) by 5 ppt relative to baseline, to act as a surrogate for the additional bromine from VLS. Recent studies have evaluated different emission inventories for VLS that utilize more detailed emission schemes than recommended for the first phase of CCMI (Hossaini et al., 2013, 2016; Lennartz et al., 2015), but model output from these recent runs are not provided in the public CCMI archive and are representative only of present time conditions. Here our focus is on the analysis of archived CCMI model simulations over long historical (1960–2010) and forecast (1960–2100) time scales conducted to study the interaction between climate change and atmospheric chemistry (Morgenstern et al., 2018; Revell et al., 2017).

## 2. Observation and Model Descriptions

### 2.1. CONTRAST and ATTREX Campaigns

Observations from the CONTRAST and ATTREX campaigns provide a comprehensive suite of chemical and physical measurements of air entering the stratosphere from the TWP. During the CONTRAST campaign, the Gulfstream V (GV) High-performance Instrument Airborne Platform for Environmental Research (HIAPER) payload collected measurements from the marine boundary layer up to 15 km (Pan et al., 2017), and during the ATTREX campaign, the NASA Global Hawk (GH) sampled air masses primarily between 14 and 20 km (Jensen et al., 2017). The Guam-based flights of CONTRAST occurred between 17 January 2014 and 24 February 2014, whereas the Guam-based phase of ATTREX took place between 12 February 2014 and 12 March 2014.

Only two CONTRAST research flights (RF), RF06 (24 January 2014) and RF15 (24 February 2014), reached the stratosphere. Consequently, data collected during RF06 and RF15 are the primary focus of this study. The GV flew north of Guam into the extratropical lowermost stratosphere (LMS) on both flights, as shown in Figure 1. Figures 1b and 1c also include a cross section of potential temperature, the pressure of the thermal tropopause (black dashed lines), and the two potential vorticity unit ( $\text{PVU} = 10^{-6} \text{ K} \cdot \text{m}^{-2} \cdot \text{kg}^{-1} \cdot \text{s}^{-1}$ ) surface (green dashed lines), for the respective flight dates. Additionally, zonal winds are shown in Figure S1 to indicate where the GV crosses the subtropical jet. These meteorological fields are from the National Center for Environmental Prediction's final (NCEP-FNL) Operational Global Analysis, which is provided every 6 hr, at  $1^\circ \times 1^\circ$  (latitude, longitude) resolution. The NCEP-FNL data were interpolated bilinearly in latitude and longitude, and linearly in time and pressure, to the GV flight track. Throughout most of this study, the GV is considered to have entered the stratosphere where it crossed the thermal tropopause, as defined by WMO (World Meteorological Organization, 1957). The sensitivity of major results to the tropopause definition is quantified in section 3.3 by also using the 2 PVU surface (i.e., the dynamical tropopause). Data collected on CONTRAST research flights other than RF06 and RF15 are also used to describe the profile of bromocarbons throughout the TWP troposphere. Tracks of these other flights are shown in Pan et al. (2017).

Measurements from the seven ATTREX flights (transit to Guam, RF01 to RF06) that sampled the stratosphere above the TWP are used. Flight tracks are shown in Figure 2. Here we only use ATTREX measurements of the nine organic compounds described in section 2.1.1 that were acquired within the TWP. We define the TWP as between latitudes of  $20^\circ\text{S}$  to  $20^\circ\text{N}$  and longitudes of  $120^\circ\text{E}$  to  $165^\circ\text{E}$ . Flight segments within the TWP are shown using blue. Figure 2b shows the GH track along with cross sections of NCEP-FNL meteorological fields for a typical ATTREX flight, RF04, which took place on 6 March 2014. In all flights, the GH provided extensive sampling within the tropical stratosphere by traveling vertically in the tropics to collect measurements above the tropical tropopause. Conversely, during CONTRAST, the GV sampled the extratropical stratosphere by flying horizontally across the subtropical jet (Figure 1).

#### 2.1.1. Aircraft Observations

The University of Miami WAS instruments collected measurements of trace gases, including CFC-11 ( $\text{CCl}_3\text{F}$ ) and bromocarbons during both ATTREX and CONTRAST (Andrews et al., 2016; Navarro et al., 2015). During

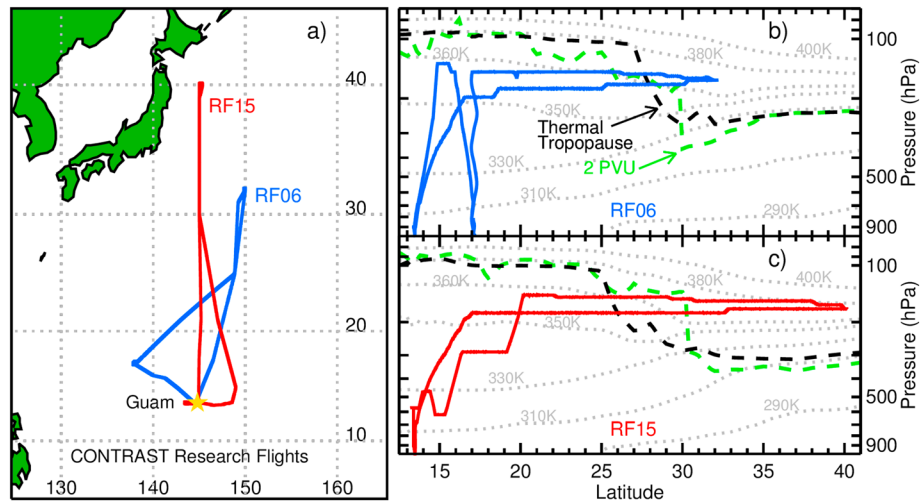


**Figure 1.** (a) Flight paths for the only two CONTRAST research flights that reached the stratosphere, RF06 and RF15. These flights were based out of Guam, indicated with a yellow star. (b) Average of the profiles of potential temperature, the 2 PVU surface, and tropopause pressure from NCEP-FNL sampled along the RF06 (24 January 2014) flight track. (c) Same as panel (b) but for RF15 (24 February 2014).

the CONTRAST campaign the WAS configuration is referred to as the Advanced WAS (AWAS), while during the ATTREX campaign, the WAS configuration is the GH WAS (GWAS). The WAS instruments collected air samples in canisters that were later analyzed using gas chromatography/mass spectrometry (GC/MS). Differences between inlet and canister systems onboard the two aircrafts are described in Andrews et al. (2016). Both sets of measurements were calibrated using the method described by Schauffler et al. (1999) and analyzed using the same GC/MS system. Our study focuses on WAS measurements of five VLS (CHBr<sub>3</sub>, CH<sub>2</sub>Br<sub>2</sub>, CH<sub>2</sub>BrCl, CHBr<sub>2</sub>Cl, and CHBrCl<sub>2</sub>), three longer-lived bromocarbons (CH<sub>3</sub>Br, halon-1211 [CBrClF<sub>2</sub>], and halon-2402 [C<sub>2</sub>Br<sub>2</sub>F<sub>4</sub>]), and CFC-11. The WAS uncertainty and limit of detection for these nine compounds are given in Table S1 of the supporting information. Overall, measurements and calibrations of VLS collected by AWAS agree well with other instruments during CONTRAST and CAST (Andrews et al., 2016).

Halon-1301 (CBrF<sub>3</sub>) was not measured during CONTRAST and ATTREX by any instrument. Therefore, computed values of halon-1301 as a function of CFC-11 from the CAM-chem-SD global model (described in section 2.1.2) are used to provide complete representation of all important organic bromine sources. Uncertainty in WAS measurements of these compounds (plus the use of modeled halon-1301 from CAM-chem-SD) are minor factors in the overall uncertainty of our scientific conclusions. Additionally, since

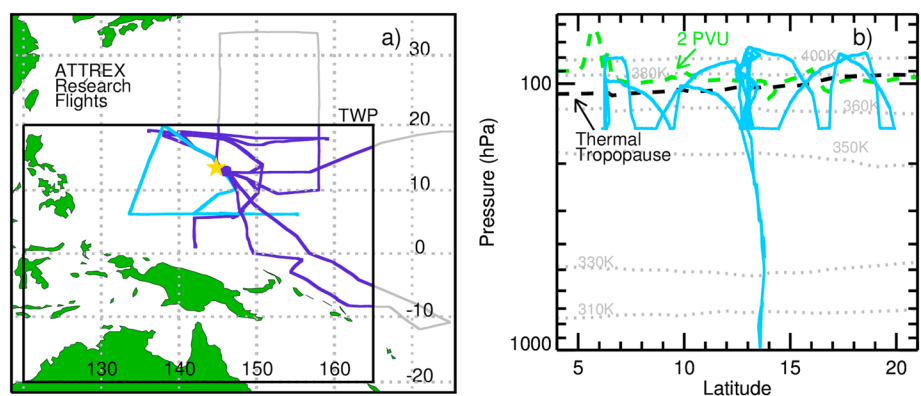


**Figure 2.** (a) Flight paths of ATTREX 2014 research flights based out of Guam (yellow star). Flight tracks within the TWP (black box) are shown as blue and outside of the TWP as grey. A specific ATTREX flight, RF04, is highlighted in light blue. (b) Average of the profiles of potential temperature, the 2 PVU surface, and tropopause pressure from NCEP-FNL sampled along the RF04 (06 March 2014) flight track.

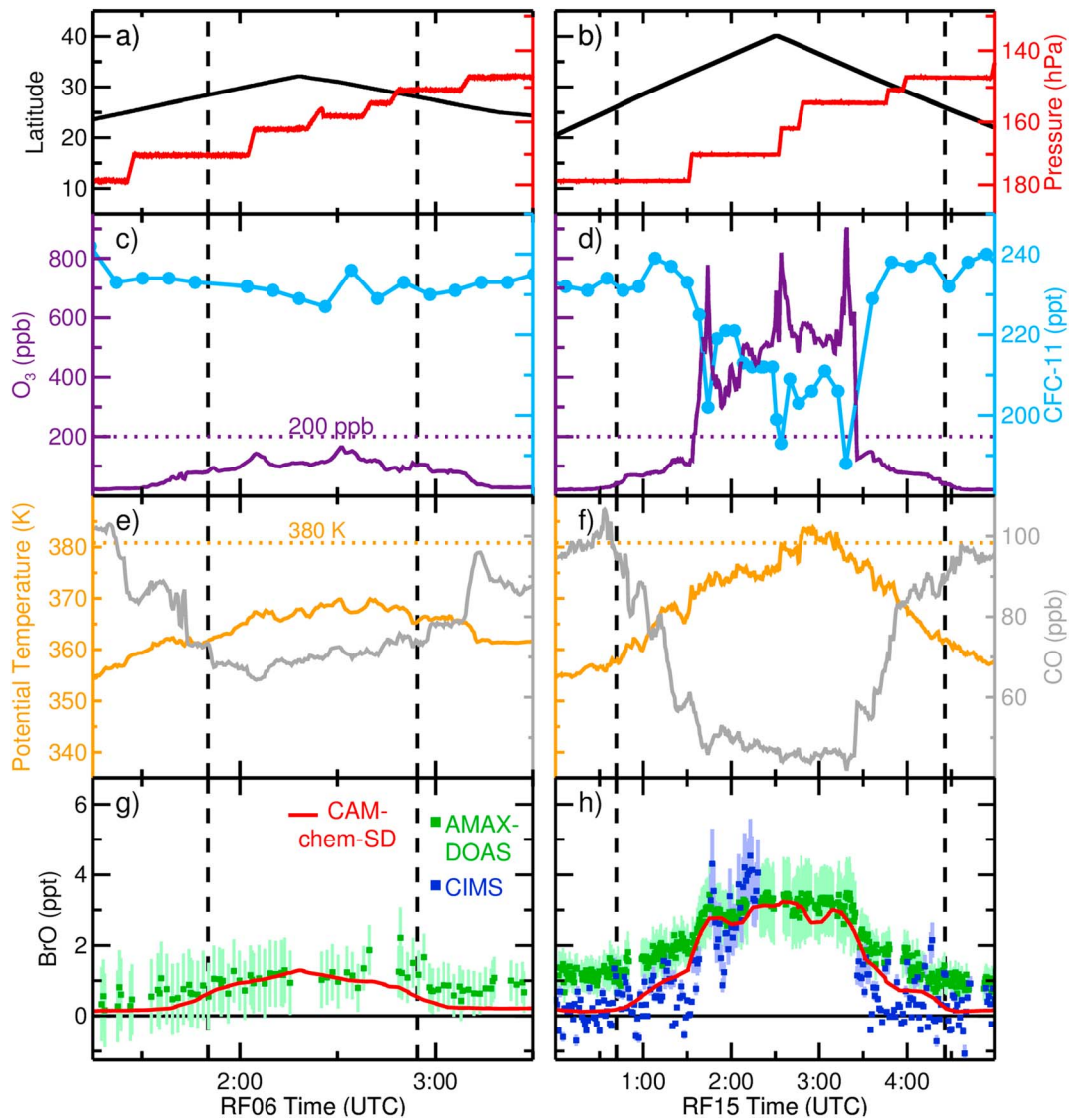


**Figure 3.** Time series of measurements obtained during CONTRAST RF06 (left column) and RF15 (right column). The black dashed vertical lines indicate when the plane crossed the NCEP-FNL thermal tropopause. (a and b) The Gulfstream V (GV) aircraft latitude (black) and pressure (red); (c and d) chemiluminescence  $O_3$  (purple) and AWAS CFC-11 (blue); (e and f) potential temperature (orange) and vacuum ultraviolet CO (grey); and (g and h) AMAX-DOAS (green) and CIMS (blue) observed BrO and CAM-chem-SD (red) modeled BrO are shown. The light green and blue bars indicate the reported  $1\sigma$  total uncertainty in AMAX-DOAS and CIMS BrO, respectively. CIMS BrO is only available for RF15 when mixing ratios of  $O_3$  are below 480 ppb (see section 2.1.1).

halon-1301 is stable within the troposphere, we expect mixing ratios at the base of the stratosphere to be similar to surface observations (Prinn et al., 2000), and there is close agreement between surface WMO measurements and CAM-chem-SD simulations (see section 3.1.2).

Measurements of CFC-11 acquired by the AWAS instrument aboard the CONTRAST GV are shown in Figure 3, for the segments of RF06 and RF15 that sampled the stratosphere. The dashed vertical lines denote crossings of the thermal tropopause. During RF06, the aircraft sampled stratospheric air only where potential temperature was below 380 K (Figure 1b), which means air masses could have entered the stratosphere through recent, isentropic transport from the tropical troposphere (Holton et al., 1995). Observed CFC-11 reached a minimum of 227 ppt, only slightly lower than the mean value of 233 ppt observed between 16.5 and 17.5 km in the TWP. During RF15, the aircraft reached air parcels with a potential temperature just above 380 K, indicative of the stratospheric overworld. Minimum CFC-11 was 188 ppt, demonstrating much deeper penetration of the stratosphere and a more photochemically aged chemical composition than sampled during RF06.

While many other chemical and physical measurements acquired by the GV HIAPER payload during RF06 and RF15 are used in our study, the time series central to our analysis are shown in Figure 3. Previous CONTRAST bromine studies (Chen et al., 2016; Koenig et al., 2017) have used the relation between mixing ratios of  $O_3$ , CO, and  $H_2O$  collected during RF15 to chemically define both the stratosphere as well as a transition layer, where there is a mixture of tropospheric and stratospheric air. While our study primarily uses the thermal tropopause, we also make use of a chemical tropopause (described below) to facilitate comparison to these two studies.

Measurements of  $O_3$  and CO are shown in Figure 3. During RF06, chemiluminescence measurements of  $O_3$  (Ridley & Grahek, 1990) peaked at 164 ppb, consistent with the indication that the plane was in the LMS based on potential temperature. For the portion of RF06 where the GV was above the thermal tropopause (between black dashed lines in Figure 3e), observations of CO, provided by an AeroLaser vacuum ultraviolet fluorescence instrument (Gerbig et al., 1999), were considerably lower than observed in the troposphere. Conversely,  $O_3$  peaked at 904 ppb on RF15, which was the deepest penetration of the stratosphere for the Guam-based flights of CONTRAST. The extremely low levels of CO observed in the middle portion of RF15 are again consistent with deep penetration of the stratosphere. During both flights, minimum mixing ratios of  $H_2O$  (not shown) measured using an open-path laser hygrometer (Zondlo et al., 2010) were around 3 ppm, characteristic of dry stratospheric air.

Koenig et al. (2017) distinguish air for which  $O_3$  is greater than 200 ppb along RF15 as the chemical stratosphere, which provides a comparable view of RF15 to the discussion in Chen et al. (2016). We also use a 200 ppb boundary because this threshold marks a sharp rise in  $O_3$  and a leveling off of the mixing ratio of CO. The two distinct relations between CO and  $O_3$  that occur on RF15, above and below where  $O_3$  is about 200 ppb, are indicative of the chemically defined stratosphere and extratropical transition layer (i.e., Gettelman et al., 2011; Pan et al., 2004, 2007).

A key component of our study is the measurement of BrO by two instruments aboard the GV during CONTRAST. The University of Colorado AMAX-DOAS instrument (Baidar et al., 2013; Dix et al., 2016; Volkamer et al., 2015) measured the differential slant column density (dSCD) of BrO and  $NO_2$  horizontally, ahead of the GV. The retrieval of dSCD and the conversion to mixing ratio for BrO and  $NO_2$  are described by Koenig et al. (2017). The AMAX-DOAS measurements of BrO and  $NO_2$  mixing ratios are reported every 30 s, as shown in Figure 3 for BrO. Since the AMAX-DOAS instrument measures ahead of the plane, we have applied a 1.8-min delay to the AMAX-DOAS observations shown in Figures 3g and 3h. Details for the calculation of this delay are given in Text S1 and Figure S2. The total measurement uncertainty for BrO and  $NO_2$  is the root sum of square combination of the dSCD fitting error and the 30% uncertainty in the volume mixing ratio conversion (Dix et al., 2016). The total error for AMAX-DOAS BrO is shown by the green error bars in Figure 3. Throughout the stratospheric portions of RF06 and RF15, the AMAX-DOAS measurement of BrO is well above the 0.4 ppt limit of detection.

The Georgia Institute of Technology CIMS instrument (Huey, 2007; Liao et al., 2011) also measured BrO during CONTRAST, as described by Chen et al. (2016). For RF01 through RF08, the use of a  $Br_2$  calibration gas interfered with these measurements, while for RF09 to RF16, a  $Cl_2$  calibration gas that posed no interference was used. As a result, CIMS observations of BrO are reported for RF15 but not RF06. Additionally, CIMS BrO is not reported where  $O_3$  is greater than 480 ppb, due to a possible instrumental interference. Our study uses CIMS 1-min measurements of BrO acquired during RF15, which have a  $1\sigma$  total measurement uncertainty of 11.5% (blue points with error bars, Figure 3h). For stratospheric air masses where  $O_3$  is below 200 ppb, CIMS BrO is frequently near or below the 0.6 ppt limit of detection (Chen et al., 2016). The CIMS instrument also reports a measurement of HOBr +  $Br_2$ , but we do not consider the observation of HOBr +  $Br_2$  in our estimates of PGI, because data for this quantity are not available where  $O_3$  mixing ratios are above 200 ppb.

The measurements of BrO from AMAX-DOAS exhibit a broad peak value of about 1 ppt for RF06 (Figure 3g). Measurements of BrO from AMAX-DOAS and CIMS peak around 3.5 and 4.5 ppt, respectively, for RF15 (Figure 3h). The largest consistent offsets between the two observations of BrO for RF15 occur on the approach and exit from the stratosphere (i.e., in the upper troposphere) and in the region of the LMS where  $O_3$  is below 200 ppb.

### 2.1.2. CAM-chem-SD

Simulations of the Community Atmosphere Model version 4 with interactive chemistry and specified dynamics (CAM-chem-SD; Tilmes et al., 2015) were prepared in support of the CONTRAST (Pan et al., 2017) and ATTREX (Jensen et al., 2017) campaigns. Dynamics were specified based on meteorological fields from the NASA Goddard Earth Observing System Model, version 5 (GEOS-5; Molod et al., 2012). Model output was prepared on a  $0.94^\circ$  latitude by  $1.25^\circ$  longitude resolution with 56 vertical levels and a 30 s temporal resolution. CAM-chem-SD simulations have been used for flight planning of both campaigns as well as post-mission data analysis (Anderson et al., 2016; Koenig et al., 2017; Navarro et al., 2015, 2017; Nicely et al., 2016).

We use output from CAM-chem-SD from a simulation that includes a detailed representation of the chemistry of bromine (Fernandez et al., 2014) and iodine (Saiz-Lopez et al., 2014) compounds, including VLSL and longer-lived bromine and chlorine sources. All five brominated VLSL measured by the WAS instruments were included in the model. Geographically resolved time-dependent marine emissions were prescribed based on a parameterization involving satellite measurements of chlorophyll-*a* (Ordóñez et al., 2012). Additional sources of inorganic bromine and chlorine through sea-salt dehalogenation as well as heterogeneous recycling reactions occurring on upper tropospheric aerosols were also considered (Fernandez et al., 2014).

Figure 3 includes time series of BrO found using CAM-chem-SD, interpolated in time and location to the GV flight tracks during CONTRAST RF06 and RF15. The BrO mixing ratios from CAM-chem-SD exhibit close agreement with the AMAX-DOAS retrieval when the GV is above the thermal tropopause during RF06 and within the chemical stratosphere ( $O_3 > 200$  ppb) during RF15. The agreement with CIMS BrO for the chemical stratosphere portion of RF15 is also very good, although there is more variability in the CIMS measurement of BrO than the AMAX-DOAS data. Sharp gradients within the chemical stratosphere are also present in the in situ measurements of  $O_3$  and CFC-11 (Figure 3d). Since AMAX-DOAS is a remote sensing instrument that measures ahead as well as in a narrow band vertically above and below the aircraft, it is possible that AMAX-DOAS observations are not able to capture the gradients in BrO observed by CIMS. However, the AMAX-DOAS observations of  $NO_2$  do reflect the sharp gradients indicated by observations of  $O_3$  (Figure S2), and the CIMS measurements have known interferences at high mixing ratios of  $O_3$  (Chen et al., 2016). As a result, in lieu of a third observation of BrO, we use measurements from both instruments in a statistical fashion to arrive at a best estimate for  $Br_y^{VLSL}$  and PGI.

For the region of the LMS where  $O_3 < 200$  ppb, the mixing ratio of BrO from CAM-chem-SD falls between the AMAX-DOAS and CIMS observations. Within this region, the CIMS observations are close or below the 0.6 ppt lower limit of detection, causing significant variability in the measurements of BrO. Additionally, Koenig et al. (2017) discuss potential reasons for the difference between CAM-chem-SD and AMAX-DOAS BrO where  $O_3 < 200$  ppb, including uncertainties in heterogeneous reaction chemistry and an additional source of  $Br_y$  from sea-salt aerosols. Difference in the two observations of BrO for this region of the LMS as well as possible shortcomings in modeled BrO supports our use of both measurements of BrO for our baseline determination of  $Br_y^{VLSL}$  and PGI in section 3.2.

### 2.2. Box Model

A photochemical steady state box model (Choi et al., 2012; Salawitch et al., 2010, 2005; Sioris et al., 2006) was used to infer gas phase  $Br_y$  from observed BrO during RF06 and RF15. The box model includes 37 chemical species and uses rate constants and absorption cross sections from the NASA Jet Propulsion Laboratory 2015 (JPL 2015) kinetic compendium (Burkholder et al., 2015) for a complete set of gas phase and heterogeneous chemical reactions known to affect stratospheric BrO. Photolysis frequencies and rate constants were calculated at the location of each AMAX-DOAS and CIMS measurement of BrO for a full diel cycle (at the latitude and pressure of the observation) in 15 min intervals. The partitioning of all species within the  $Br_y$  family was found assuming photochemical steady state over the diel cycle. The modeled BrO/ $Br_y$  ratio for the local solar time of each measurement of BrO was then used to infer  $Br_y$  along the tracks of RF06 and RF15. Our analysis of  $Br_y$  inferred from BrO is restricted to measurements obtained in the stratosphere, as defined by either the thermal or dynamical tropopause.

The box model was constrained to a wide range of GV HIAPER observations, listed in Table 1. One-minute averages of GV HIAPER measurements of temperature, pressure,  $O_3$ , CO,  $CH_4$ , and  $H_2O$  were used to constrain the box model. Additionally, surface reflectivity in the model was scaled so that the modeled photolysis



**Table 1**
*The GV HIAPER Measurements, Collected During CONTRAST RF06 and RF15, Used to Constrain the Steady State Box Model*

Instrument	Measurement	Reference
Airborne Multiaxis DOAS (AMAX-DOAS)	NO <sub>2</sub> (NO <sub>y</sub> )	Koenig et al. (2017)
Advanced Whole Air Sampler (AWAS)	CFC-11 (Cl <sub>y</sub> )	Schauffler et al. (2003)
Chemiluminescence	O <sub>3</sub>	Ridley and Grahek (1990)
HIAPER Airborne Radiation Package (HARP)	J(NO <sub>2</sub> ) and J(O <sub>3</sub> → O( <sup>1</sup> D))	Shetter and Müller (1999)
Picarro	CH <sub>4</sub>	Crosson (2008)
Open Path Hygrometer	H <sub>2</sub> O	Zondlo et al. (2010)
Ultra-High Sensitivity Aerosol Spectrometer (UHSAS)	Aerosol surface area density	Cai et al. (2008)
AeroLaser vacuum ultraviolet	CO	Gerbig et al. (1999)

frequency of NO<sub>2</sub> ( $J_{\text{NO}_2}$ ) matched the observation of  $J_{\text{NO}_2}$  from the HARP instrument. Similarly, total column O<sub>3</sub> was scaled to force agreement between modeled and measured photolysis frequency of O<sub>3</sub>, producing O(<sup>1</sup>D),  $J_{\text{O}_3 \rightarrow \text{O}(\text{1D})}$ . All other  $J$ -values were calculated using these HARP-based estimates of surface reflectivity and total column O<sub>3</sub>. The number distribution of particles with diameters between 0.06 and 1 μm was measured using an Ultra-High Sensitivity Aerosol Spectrometer (UHSAS; Cai et al., 2008). Aerosol surface area density (SAD) was calculated from UHSAS measurements assuming spherical sulfate particles. Due to variability in the aerosol SAD calculated from UHSAS measurements, the box model was constrained to the 5-min running mean of aerosol SAD (Figure S3). We treat all aerosols as sulfate, since the temperature was well above the frost point during all stratospheric observations. We have also specified inorganic chlorine (Cl<sub>y</sub>) along the GV tracks of RF06 and RF15 using AWAS measurements of CFC-11, tied to the relation between CFC-11 and Cl<sub>y</sub> computed within CAM-chem-SD for the latitudes and longitudes of both flights (Figure S4). Based on our analysis, presented in section 3.2, this estimate introduces only a minor uncertainty in inferred Br<sub>y</sub>.

Chemiluminescence measurements of both NO and NO<sub>2</sub> were acquired during CONTRAST. However, this measurement of NO<sub>2</sub> is believed to have been influenced by an unknown amount of thermally decomposed nitrogen compounds, which leads to an overestimate in the upper troposphere and stratosphere due to the cold conditions of ambient air. Since the modeled BrO/Br<sub>y</sub> ratio is sensitive to the trimolecular reaction between BrO and NO<sub>2</sub> (see section 3.2), total nitrogen oxides (NO<sub>y</sub>) in the box model have been scaled to match the mixing ratio of NO<sub>2</sub> reported by the AMAX-DOAS instrument. However, the use of chemiluminescence NO rather than AMAX-DOAS NO<sub>2</sub> as a model constraint indicates a lower abundance of NO<sub>2</sub> (blue line in Figure S2), thereby lowering the amount of Br<sub>y</sub> inferred from the observed BrO. As a result, we examine uncertainty in modeled Br<sub>y</sub> by also constraining the model to the observed mixing ratio of NO, since the chemiluminescence measurement of NO is unaffected by thermally labile nitrogen compounds due to the design of the instrument. Because NO<sub>2</sub> provides a more direct constraint for the BrO/Br<sub>y</sub> ratio, we use AMAX-DOAS NO<sub>2</sub> in our baseline simulations.

The value of Br<sub>y</sub> consistent with each observation of BrO along RF06 and RF15 was found in an iterative fashion. The box model was initialized with Br<sub>y</sub> from CAM-chem-SD. Box-modeled Br<sub>y</sub> was then adjusted so that box-modeled BrO matched either AMAX-DOAS or CIMS BrO, to within 2%. Analysis of Br<sub>y</sub> found in this manner is limited to the stratosphere (i.e., region between the black vertical dashed lines of Figure 3). The effects on computed Br<sub>y</sub> of kinetic and measurement uncertainties are considered in section 3.2 by applying a 1σ displacement in the JPL 2015 uncertainty for the rates of the eight most important chemical reactions that govern the BrO/Br<sub>y</sub> ratio and by adjusting model inputs according to their 1σ uncertainty (Table S2).

### 3. Results and Discussion

#### 3.1. Organic Bromine

##### 3.1.1. Organic Bromine Tracer Relations

Stratospheric tracer-tracer relations were developed using simultaneous WAS measurements of bromocarbons and CFC-11. The use of a stratospheric tracer, such as CFC-11, allows bromocarbons to be analyzed as a function of photochemical aging in the stratosphere (Wamsley et al., 1998) and provides a convenient means for comparing field measurements with the output of global models (e.g., Kovalenko et al., 2007;

**Table 2**  
Fitting Parameters for the Stratospheric Tracer-Tracer Relation Between Bromocarbons and CFC-11 (Equation (1))

	CBr <sub>y</sub>	WMO lifetime <sup>a</sup>	(X) <sub>o</sub> (ppt)	<i>d</i>	Source
Long-lived	CH <sub>3</sub> Br	26.3 years	7.20 ± 0.21	0.77 ± 0.09	CONTRAST
	CBrClF <sub>2</sub> (halon-1211)	41	3.72 ± 0.09	0.66 ± 0.06	CONTRAST
	CBrF <sub>3</sub> (halon-1301)	73.5	3.24 ± 0.06	1.265 ± 0.001	CAM-chem-SD
	C <sub>2</sub> Br <sub>2</sub> F <sub>4</sub> (halon-2402)	41	0.81 ± 0.03	0.73 ± 0.08	CONTRAST
	SGI <sup>LL</sup>		15.0 ± 0.2		
VSLS	CH <sub>2</sub> Br <sub>2</sub>	150 days	1.36 ± 0.42	0.10 ± 0.03	CONTRAST
	CHBr <sub>3</sub>	17	1.01 ± 0.47	0.05 ± 0.01	ATTREX
	CHBrCl <sub>2</sub>	48	0.24 ± 0.07	0.06 ± 0.01	ATTREX <sup>b</sup>
	CHBr <sub>2</sub> Cl	28	0.20 ± 0.08	0.06 ± 0.01	ATTREX
	CH <sub>2</sub> BrCl	174	0.11 ± 0.03	0.12 ± 0.03	CONTRAST
	SGI <sup>VLS</sup>		2.9 ± 0.6		

Note. All mixing ratios are multiplied by the bromine atomicity. The value for (CFC-11)<sub>o</sub> is 233 ppt and is calculated from the mean of ATTREX observations at 17 km in the TWP. The stratospheric lifetime of CFC-11 is 52 years.

<sup>a</sup>The WMO 2014 lifetimes for long-lived compounds are the stratospheric partial lifetimes and for VSLS are the 10 km tropical lifetimes. <sup>b</sup>For CHBrCl<sub>2</sub>, (X)<sub>o</sub> is the ATTREX TWP mean at 17 km, and *d* is estimated from observations of CHBr<sub>2</sub>Cl.

Salawitch et al., 2005, 2010). Our study uses measurements of CFC-11 and eight bromocarbons to estimate how much Br<sub>y</sub> should have formed as a result of the stratospheric decay of both VSLS and longer-lived bromocarbons.

Our procedure for calculating the tracer-tracer relations follows Wamsley et al. (1998). The decay of a long-lived bromocarbon, denoted as (X), in relation to decay of CFC-11 can be represented as

$$(X) = (X)_o \left[ \frac{(CFC - 11)}{(CFC - 11)_o} \right]^{\frac{1}{d}} \quad (1)$$

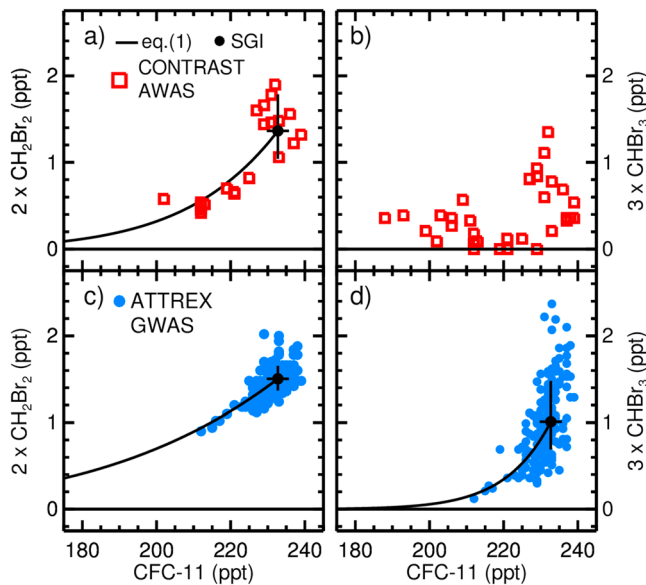
where (X)<sub>o</sub> and (CFC-11)<sub>o</sub> represent the tropical tropopause mixing ratios. For long-lived compounds, such as halons, the decay parameter *d* in equation (1) is equal to the ratio of the lifetimes (τ) of the bromocarbon relative to CFC-11 (i.e.,  $d = \tau_X / \tau_{CFC - 11}$ ; Plumb & Ko, 1992). However, discrepancies between the observed decay parameter *d* and the ratio of the lifetimes have been observed for shorter-lived compounds, including CH<sub>3</sub>Br (Avallone & Prather, 1997; SPARC, 2013).

Table 2 contains fitting parameters used to define tracer-tracer relations central to our analysis. For our primary analysis of aircraft data, we have taken the logarithm of equation (1), which leads to

$$\ln(X) = \frac{1}{d} \ln \left[ \frac{(CFC - 11)}{(CFC - 11)_o} \right] + \ln(X)_o \quad (2)$$

and solved for *d* and (X)<sub>o</sub> using linear least squares analysis of simultaneous measurements of each bromocarbon and CFC-11. The value for (CFC-11)<sub>o</sub> was set to 233 ppt throughout our study, based on the mean of all ATTREX observations of CFC-11 obtained at 17 km altitude (i.e., between 16.5 and 17.5 km) by the GWAS instrument in the TWP. The use of data collected at 17 km to define the abundance of CFC-11 at the base of the stratosphere is also consistent with the approach used in WMO 2014 (Carpenter et al., 2014) and other estimates of SGI (i.e., Navarro et al., 2015) because the cold-point tropopause, used to denote the top of the TTL, lies close to 17 km in the tropics. Since many of the bromocarbon compounds have short tropospheric lifetimes, resulting in large seasonal and geographic gradients, solving for (X)<sub>o</sub> using equation (2) is more representative of entry into the global stratosphere than values of (X)<sub>o</sub> based on ATTREX measurements at 17 km within the TWP. Comparison of (X)<sub>o</sub> from these two methods is given in section 3.1.2. For Table 2 and throughout, we report values of (X)<sub>o</sub> as the mixing ratio multiplied by the bromine atomicity in each compound, since the sum of bromine atoms is used to define SGI. The lifetime of each VSLS at 10 km altitude in the tropics, from Table 1–5 of WMO 2014, is also given for each VSLS.

The relations between the two major VSLS (CH<sub>2</sub>Br<sub>2</sub> and CHBr<sub>3</sub>) and CFC-11, observed during CONTRAST and ATTREX, are shown in Figure 4. Similar plots for the minor VSLS (CH<sub>2</sub>BrCl, CHBr<sub>2</sub>Cl, and CHBrCl<sub>2</sub>) are shown in Figure S5, and all fitting parameters calculated using ATTREX observations are given in Table S3. Figures 4a and 4b show data collected in the extratropical stratosphere during RF06 and RF15 of CONTRAST, whereas



**Figure 4.** Stratospheric observations of VSLS as function of CFC-11. The solid lines are linear fits to the observations found using equation (2). The black points are SGI of each compound, also calculated using equation (2). The horizontal error bars are the standard deviation the ATTREX measurements of CFC-11 between 16.5 and 17.5 km. The vertical error bars are the uncertainty in the fit where CFC-11 is 233 ppt. (a) CONTRAST AWAS measurements of  $\text{CH}_2\text{Br}_2$  and CFC-11 collected in the extratropical stratosphere. (b) CONTRAST AWAS measurements of  $\text{CHBr}_3$  and CFC-11; the short lifetime of  $\text{CHBr}_3$  combined with presumably rapid horizontal transport of the LMS air masses, sampled during CONTRAST, prevents the calculation of a meaningful fit. (c) ATTREX GWAS observations of  $\text{CH}_2\text{Br}_2$  and CFC-11 in the TWP; (d) ATTREX GWAS observations of  $\text{CHBr}_3$  and CFC-11 in the TWP.

relative to CFC-11 in the extratropical stratosphere can be adequately described using equation (1). As expected, these compounds exhibit more scatter versus CFC-11 than observed for longer-lived halons (Figure S6), but a reasonable fit can be achieved. Since the three shortest-lived VSLS ( $\text{CHBr}_3$ ,  $\text{CHBr}_2\text{Cl}$ , and  $\text{CHBrCl}_2$ ) are more sensitive to local chemical environments, meaningful fits could not be determined for CONTRAST observations of these VSLS in the LMS (Figures 4b and S5).

Consequently, Table 2 contains entries for fitting parameters of five VSLS, from a mixture of CONTRAST and ATTREX observations. Together, minor VSLS supply 0.6 ppt to the stratosphere in comparison to  $\text{CHBr}_3$  and  $\text{CH}_2\text{Br}_2$ , which supply a combined 2.4 ppt. Careful consideration for  $\text{CHBrCl}_2$  was necessary, because WAS observations were sparse at low mixing ratios of CFC-11 during both CONTRAST and ATTREX. For this species, we used the mean value of  $\text{CHBrCl}_2$  observed at 17 km (i.e., between 16.5 and 17.5 km) in the TWP during ATTREX to define  $(X)_o$ . Since the lifetime of  $\text{CHBrCl}_2$  is closest to the lifetime of  $\text{CHBr}_2\text{Cl}$ , the decay parameter from the  $\text{CHBr}_2\text{Cl}$  fit was used.

Finally, Table 2 also shows fitting parameters for the four long-lived bromocarbons (Figure S6) that have traditionally been considered in studies of stratospheric ozone depletion and recovery. For reference, Table 2 also lists the stratospheric lifetimes of these compounds, obtained from Table 1–3 of WMO 2014, originally reported in SPARC (2013). Data acquired in the stratosphere on CONTRAST RF06 and RF15 are used, except for halon-1301, which was not measured during either CONTRAST, ATTREX, or CAST. The fit parameters for halon-1301 are based on analysis of output from CAM-chem-SD along RF06 and RF15 of CONTRAST. The fits conform to prior expectation (Wamsley et al., 1998) and yield a value of  $15.0 \pm 0.2$  ppt for the sum of the four values of  $(X)_o$ , which means 15.0 ppt of bromine was delivered to the

**Table 3**

Mean Mixing Ratios Between 16.5 and 17.5 km From ATTREX and WMO 2014

VSLS	ATTREX TWP 17 km mean (ppt)	WMO 2014 tropical 17 km mean (ppt)
$\text{CH}_2\text{Br}_2$	$1.56 \pm 0.10$	1.06 (0.6–1.72)
$\text{CHBr}_3$	$1.21 \pm 0.23$	0.24 (0.00–0.93)
$\text{CHBrCl}_2$	$0.24 \pm 0.07$	0.06 (0.03–0.12)
$\text{CHBr}_2\text{Cl}$	$0.22 \pm 0.05$	0.04 (0.00–0.28)
$\text{CH}_2\text{BrCl}$	$0.12 \pm 0.02$	0.07 (0.05–0.11)
$\text{SGI}^{\text{VSLS}}$	$3.4 \pm 0.3$	1.4 (0.7–3.4)

Note. All mixing ratios are multiplied by the bromine atomicity.

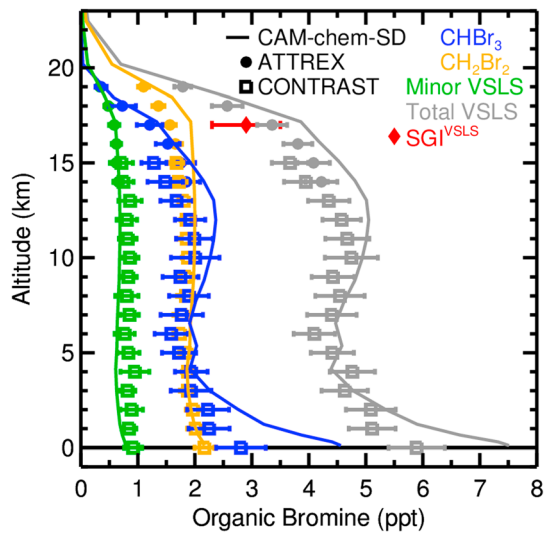


**Figure 5.** Profiles of VSLs in the TWP during winter 2014. Observations have been sorted into 1 km altitude bins, and all quantities represent mixing ratios multiplied by bromine atomicity. Square points are CONTRAST AWAS means, circle points are ATTREX GWAS means, and error bars are the standard deviation of data within each bin (various colors as indicated). The solid lines are average CAM-chem-SD profiles in the TWP. Minor VSLs (green) is the sum of  $\text{CH}_2\text{BrCl}$ ,  $\text{CHBr}_2\text{Cl}$ , and  $\text{CHBrCl}_2$ , and total VSLs (grey) is the sum of minor VSLs,  $\text{CHBr}_3$ , and  $\text{CH}_2\text{Br}_2$ . The red diamond is  $\text{SGI}^{\text{VSLs}}$  calculated from CFC-11 tracer relations,  $2.9 \pm 0.6$  ppt (Table 2).

CONTRAST and ATTREX, respectively. The WAS measurements have been averaged within 1 km altitude bins, and the error bars represent the standard deviation about the mean within each bin. CONTRAST data shown in Figure 5 were acquired during 12 flights in the TWP, including portions of RF06 and RF15. The lines show calculations of profiles for these VSLs, averaged for February over the TWP, from CAM-chem-SD (Fernandez et al., 2014; Navarro et al., 2015; section 2.1.2). Note that the three minor VSLs have been summed together, for both measured and modeled profiles. Comparatively, the red diamond represents the tracer-based estimate for  $\text{SGI}^{\text{VSLs}}$  of  $2.9 \pm 0.6$  ppt, described above.

Overall the observed vertical profiles of VSLs from CONTRAST and ATTREX compare well to modeled profiles from CAM-chem-SD in the TTL. Navarro et al. (2015) showed similarly good comparisons, based on ATTREX observations in the Western and Eastern Pacific. The CAM-chem-SD profile is slightly higher than observed for  $\text{CH}_2\text{Br}_2$  above 15 km and for  $\text{CHBr}_3$  between 11 and 14 km, leading to slightly larger modeled values for  $\text{CBr}_y$  than observed in the TTL ( $\sim 13$  to 17 km). Below 2 km,  $\text{CHBr}_3$  mixing ratios are higher in CAM-chem-SD than the mean values observed during CONTRAST (Figure 5). A similar discrepancy exists between CAM-chem-SD  $\text{CHBr}_3$  and measurements obtained during CAST (not shown), which sampled altitudes below 8 km in the TWP during winter 2014 (Andrews et al., 2016). Previous evaluations of the Ordóñez et al. (2012) climatology, used by CAM-chem-SD for emissions of VSLs, have identified the potential to overestimate the actual emissions of  $\text{CHBr}_3$  based on a comparison of model output to ground-based and Southeast Asian aircraft observations (Hossaini et al., 2013, 2016). However, CAM-chem-SD shows very good agreement with ATTREX measurements of  $\text{CHBr}_3$  sampled at higher altitudes. Vertical profiles of all individual VSLs and longer-lived compounds are shown in Figure S8. In this figure, WMO 2014 surface mixing ratios of  $\text{CH}_3\text{Br}$ , halons, and CFC-11 are included (Harris et al., 2014), demonstrating good agreement between CAM-chem-SD tropospheric and WMO 2014 surface values for all compounds.

As noted above, some prior estimates of  $\text{SGI}^{\text{VSLs}}$  have been based on observations near 17 km. For this altitude in the TWP, the bromine content of the five VSLs observed during ATTREX is  $3.4 \pm 0.3$  ppt (Table 3). This estimate differs slightly from the value of  $3.27 \pm 0.47$  ppt reported by Navarro et al. (2015), because we have restricted our analysis to GWAS measurements collected within  $20^\circ\text{S}$  to  $20^\circ\text{N}$ . A comparison to the prior estimates of VSLs at 17 km in the tropics, given in Chapter 1 of WMO 2014,

stratosphere by long-lived sources in winter 2014. This estimate is in agreement with the WMO 2014 time series for the delivery of bromine to the stratosphere by these four compounds (Figure S7). Finally, the product of the decay parameter for the various halons and the WMO 2014 estimate of 52 years for the stratospheric lifetime for CFC-11 results in computed lifetimes of 34, 66, and 38 years, respectively, for halon-1211, -1301, and -2404. These values are slightly lower than but consistent with the stratospheric partial lifetimes reported by WMO 2014, given in Table 2.

### 3.1.2. Source Gas Injection From VSLs ( $\text{SGI}^{\text{VSLs}}$ )

An important focus of CONTRAST and ATTREX was the quantification of the stratospheric supply of bromine via both SGI and PGI. Here we used the fits of VSLs as functions of CFC-11 (Table 2) to arrive at an estimate for  $\text{SGI}^{\text{VSLs}}$  of  $2.9 \pm 0.6$  ppt. The value of 2.9 ppt is the sum of the five values of  $(X)_o$  for VSLs, and the uncertainty of 0.6 ppt is a root sum of squares combination of the fitting uncertainties for the five VSLs. This estimate combines data acquired at the top of the TTL and within the photochemically aged stratosphere in the context of a physically plausible model for the decay of the bromocarbons and mimics the approach of Wamsley et al. (1998). An alternate method to estimate  $\text{SGI}^{\text{VSLs}}$  is to tabulate the bromine content of the five VSLs compounds near 17 km in the tropics, which we quantify below.

Figure 5 shows vertical profiles of VSLs in the TWP and compares these two approaches for estimating  $\text{SGI}^{\text{VSLs}}$ . The square and circle symbols represent the organic bromine content of various VSLs measured during

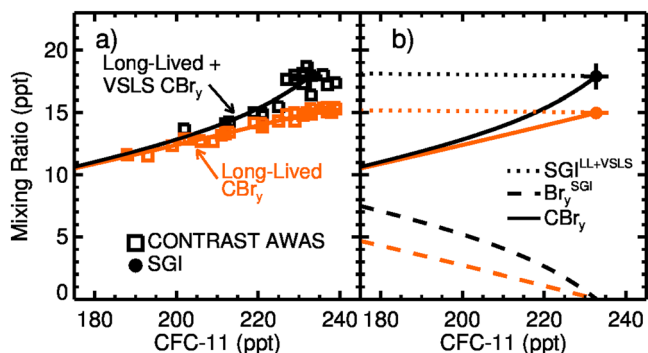


**Figure 6.** Stratospheric tracer relations between bromine and CFC-11 in winter 2014. In both panels, orange is the sum of bromine supplied by only long-lived compounds ( $CH_3Br$  and halons), and black is the sum of bromine supplied by long-lived compounds and VLSL. The circle points and error bars are the mean and standard deviation of  $CBr_y$  and CFC-11 at the base of the stratosphere (i.e., CFC-11 = 233 ppt). (a) The solid lines are the calculated relation between  $CBr_y$  and CFC-11 from CONTRAST and ATTREX observations (Table 2). The squares represent the sum of CONTRAST measurements of bromocarbons collected during RF06 and RF15. (b)  $Br_y^{SGI}$  (dashed lines) calculated from the difference between  $CBr_y$  (solid lines) and  $SGI^{LL+VLSL}$  (dotted lines) using equation (4).

seven flights of the GH during ATTREX, it is unclear how representative the measurements acquired at 17 km are of the conditions for the entire winter in the TWP. Furthermore,  $SGI^{VLSL}$  sampled over the TWP during the biologically and convectively active boreal winter may be high with respect to the tropical average. Due to their short lifetimes, the transport of VLSL is expected to be highly variable in both time and space. For instance, the CONTRAST campaign sampled the TTL in the TWP earlier in the winter season compared to ATTREX (Jensen et al., 2017; Pan et al., 2017). For the overlapping altitude region of these two data sets (i.e., between 14 and 15 km), the CONTRAST observations of the bromine content of VLSL in the TWP are 0.3 ppt lower than measured during ATTREX. This offset is largely due to lower  $CHBr_3$  mixing ratios measured during CONTRAST than ATTREX (Figures 5 and S8). Since AWAS and GWAS measurements use the same calibration and GC/MS systems (Andrews et al., 2016), this difference probably indicates that for the conditions sampled during CONTRAST, there was either slightly smaller emissions or less efficient vertical transport of  $CHBr_3$  than occurred for the air masses sampled later in winter at 17 km during ATTREX.

We use the tracer-based value for  $SGI^{VLSL}$  of  $2.9 \pm 0.6$  ppt in the analysis below. Given the short lifetimes of many VLSL, we place greater emphasis on this estimate of  $SGI^{VLSL}$ , since this method inherently includes air parcels with a much greater diversity of convective histories than estimates based only on observations near 17 km in the TWP. For instance, the tracer-based estimates of SGI from  $CHBr_3$  and  $CH_2Br_2$  (Table 2) are both about 0.2 ppt lower than their 17 km means (Table 3). The tracer analysis for  $CHBr_3$  is based on all stratospheric ATTREX measurements in the TWP, which includes measurements around 17 km as well as more convectively aged air parcels at higher altitudes. Additionally, the tracer-based estimate for SGI of  $CH_2Br_2$  makes use of data that span a large range of latitudes and provides a more direct representation of the conditions sampled by the instruments that measured BrO, which is used to calculate PGI.

### 3.1.3. Inorganic Bromine From SGI ( $Br_y^{SGI}$ )

The bromocarbon versus CFC-11 tracer relations, defined in section 3.1.1, are used to calculate the expected formation of  $Br_y$  following stratospheric decay of VLSL,  $CH_3Br$ , and halons, which we term  $Br_y^{SGI}$ . Figure 6 illustrates our approach for estimating the expected rise of  $Br_y^{SGI}$  as a function of decay of CFC-11. This estimate of  $Br_y^{SGI}$  is an essential component for a comprehensive analysis of the bromine budget for the TWP. Here we combine the estimate of  $Br_y^{SGI}$  with a box model analysis of measured BrO to infer PGI from VLSL (section 3.2).

Figure 6a shows the relation between stratospheric  $CBr_y$  (i.e., carbon-bonded bromine) and CFC-11, calculated according to

shows that ATTREX observations of  $CH_2Br_2$ ,  $CH_2BrCl$ , and  $CHBr_2Cl$  all lie within the WMO 2014 range (0.7 to 3.4 ppt), albeit on the upper end (Table 3). The ATTREX determination of  $SGI^{VLSL}$  in the TWP of  $3.4 \pm 0.3$  ppt is, however, more than a factor of 2 greater than the WMO 2014 best estimate of 1.4 ppt. Furthermore, the ATTREX 17 km mean observations of  $CHBr_3$  and  $CHBrCl_2$  exceed the upper range from WMO 2014. This difference could be due to our sampling of the biologically and convectively active TWP, since the WMO 2014 average values are based on measurements throughout the tropics. Additionally, the mean and standard deviation of AWAS measurements of VLSL between 10 and 12 km is  $4.7 \pm 0.6$  ppt. This value is slightly higher than but within one standard deviation of previously reported upper tropospheric VLSL of  $4.4 \pm 0.4$  ppt (Sala et al., 2014) and  $4.2 \pm 0.6$  ppt (Wisher et al., 2014) that are based on aircraft observations collected above Southeast Asia. Recently, Fiehn et al. (2018) have emphasized that considerable seasonal and interannual variability in  $SGI^{VLSL}$  could be expected.

The upper limit for the uncertainty in our  $2.9 \pm 0.6$  ppt tracer-based estimate for  $SGI^{VLSL}$  (red diamond in Figure 5) encompasses the value of  $SGI^{VLSL}$  measured at 17 km during ATTREX ( $3.4 \pm 0.3$  ppt, grey circle at 17 km in Figure 5). Despite the coverage of observations provided by

$$CBr_y = \sum (X_i)_o \left[ \frac{(CFC - 11)}{(CFC - 11)_o} \right]^{\frac{1}{d_i}} \quad (3)$$

where the summation is performed over all bromocarbons, indicated by  $i$ . The two lines in Figure 6a make use of values of  $(X_i)_o$  and  $d_i$  given in Table 2. Here and throughout, orange is used to represent the stratospheric supply of bromine from only  $CH_3Br$  and halons, while black is used to represent the supply from both VLSL and long-lived compounds. The solid lines show the slow decay of the bromocarbons in the LMS, as CFC-11 decreases, represented by equation (3). The squares indicate the total organic bromine content as measured by AWAS during CONTRAST, plus the CAM-chem-SD value for halon-1301. In some instances, the measurements from AWAS are incomplete (i.e., the mixing ratio for one or more of the eight AWAS compounds in Table 2 is not available). If values for either  $CHBrCl_2$  or halon-1211 are missing, we used the fit parameters to estimate the abundance. This allows for more data points on Figure 6a.

Figure 6b illustrates our estimate for the appearance of inorganic bromine upon stratospheric oxidation of the organic sources, following the approach of Wamsley et al. (1998). Assuming that the total bromine content of the stratosphere is present either in organic or inorganic form in the gas phase (i.e., aerosol uptake and washout, within the stratosphere, are inconsequential), then the inorganic bromine ( $Br_y^{SGI}$ ) provided by the oxidation of organics is represented by:

$$Br_y^{SGI} = SGI^{LL+VLSL} - CBr_y \quad (4)$$

where  $CBr_y$  is calculated according to equation (3). In equation (4),  $SGI^{LL+VLSL}$  is the total bromine that entered the stratosphere in organic form: that is,  $SGI^{LL+VLSL}$  equals the sum of SGI from long-lived compounds ( $SGI^{LL}$ ) and  $SGI^{VLSL}$ .

We assume that the value of  $SGI^{VLSL}$  measured during CONTRAST and ATTREX campaigns is constant over time. Conversely, it is known that  $SGI^{LL}$  varies over time, and the surface mixing ratios of  $CH_3Br$  and halons have decreased slightly over the past decade due to the success of the Montreal Protocol (Figure S7). In order to represent the slow decay of  $CH_3Br$  and halons in the global troposphere, an estimate for the age of stratospheric air is needed. Age of air is the mean time an air parcel takes to travel from the base of the stratosphere to the location of measurement (Hall & Plumb, 1994). Here the  $N_2O$ -based estimate for age of air given in Engel et al. (2002) is used, tied to the CFC-11 versus  $N_2O$  relation from CAM-chem-SD and AWAS observations of CFC-11 (see Text S2 in the supporting information). The mean age of air as a function of CFC-11 has been used to adjust  $SGI^{LL}$  in Figure 6b, such that the values correspond to the time series of  $CH_3Br$  and halon surface mixing ratios given in Chapter 5 of WMO 2014 (Harris et al., 2014). The bromine content of  $SGI^{LL}$ , represented by the orange dotted line in Figure 6b, increases slightly from 15.0 ppt where CFC-11 is 233 ppt to 15.2 ppt where CFC-11 is 175 ppt, which reflects the slow, gradual decline of long-lived bromocarbons.

Finally, the dashed lines in Figure 6b represent the rise in inorganic bromine due to the decay of long-lived bromocarbons as a function of CFC-11 (orange) and the rise in organic bromine due to the decay of all sources that enter the stratosphere with carbon intact (black;  $Br_y^{SGI}$ ). The curve for  $Br_y^{SGI}$  was found using equation (4); in simple graphical terms,  $Br_y^{SGI}$  is the difference between the black dotted and the black solid lines in Figure 6b. Similarly, the orange dashed line is the difference between the orange dotted and solid lines.

### 3.2. Product Gas Injection (PGI)

Here we estimate the supply of bromine to the stratosphere by inorganic species that cross the tropopause. The estimate of PGI given below is unable to distinguish between inorganic bromine produced following the decomposition of VLSL and inorganic bromine from other sources, such as sea-salt aerosol. While theoretically sea-salt aerosol should be most important in the lower portions of the tropical troposphere, a number of recent studies have shown that this source can be important at higher altitudes, mainly within regions of active convective such as the TWP (Fernandez et al., 2014; Koenig et al., 2017; Long et al., 2014; Schmidt et al., 2016; Wang et al., 2015; Yang et al., 2005).

Figures 7a and 7b show the partitioning of gas phase  $Br_y$  compounds within our constrained photochemical box model (section 2.2) along each of the CONTRAST flight tracks. Figures 7c and 7d display the time series of gas phase  $Br_y$  inferred from observations of BrO reported by AMAX-DOAS (green) and CIMS (blue) for

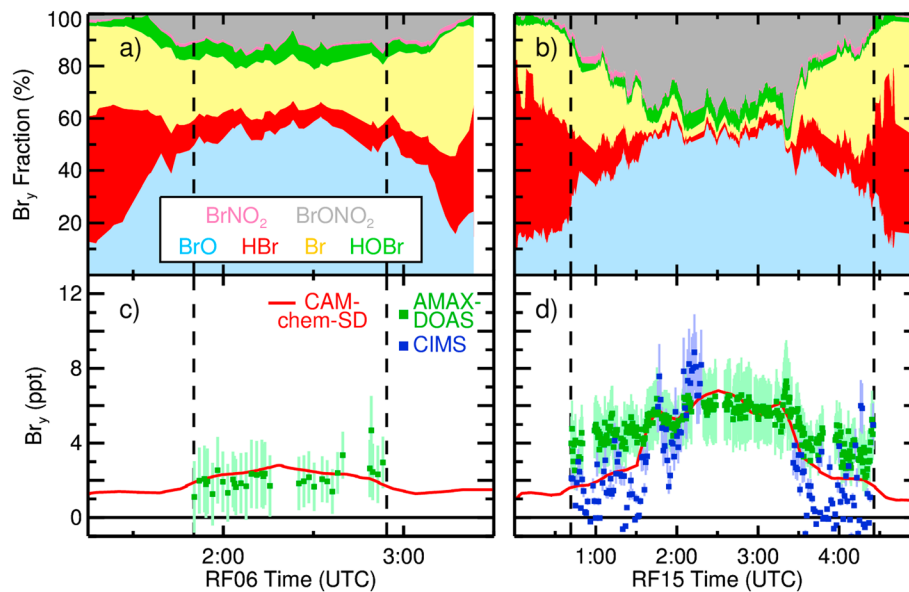


**Figure 7.** Model output and inferred  $Br_y$  for CONTRAST RF06 (left column) and RF15 (right column). In all panels, the black vertical dashed lines indicate when the plane crossed the tropopause. (a and b)  $Br_y$  partitioning within the box model for the local solar time of aircraft observations. (c and d)  $Br_y$  inferred using the box modeled  $BrO/Br_y$  ratio as well as AMAX-DOAS (green) and CIMS (blue)  $BrO$  observations. The error bars represent  $BrO$  measurement uncertainties, multiplied by the modeled  $Br_y/BrO$  ratio. The red lines are CAM-chem-SD modeled  $Br_y$  interpolated to the respective flight tracks.

CONTRAST RF06 and RF15. The error bars for  $Br_y$  in these panels were calculated by applying the box model  $BrO/Br_y$  partitioning to the upper and lower  $1\sigma$  uncertainty limits of the  $BrO$  measurements reported by the two instruments teams. The value of  $Br_y$  within CAM-chem-SD, interpolated in space and time to the GV flight tracks, is shown by the red lines. As the GV entered the stratosphere (black vertical dashed lines),  $Br_y$  increases as expected. The value of  $Br_y$  inferred from AMAX-DOAS  $BrO$  broadly peaked around 3 ppt for RF06, and  $Br_y$  inferred from both AMAX-DOAS and CIMS  $BrO$  peaks around 6 ppt for RF15. As noted in section 2.1.1, observations of  $BrO$  from CIMS are not available for RF06. The rise in  $Br_y$  is considerably more pronounced for RF15, reflecting deeper penetration into the stratosphere. The simulation of  $Br_y$  from CAM-chem-SD exhibits overall good agreement with  $Br_y$  inferred from  $BrO$  and related observations during the middle portion of RF15 where the aircraft sampled deeper in the stratosphere, and mixing ratios of  $O_3$  are above 200 ppb.

The largest difference between  $Br_y$  inferred from AMAX-DOAS and CIMS occurs near the edges of the stratosphere (Figure 7d). The CAM-chem-SD value for  $Br_y$  nearly splits the difference between the estimates based on AMAX-DOAS and CIMS  $BrO$ , similar to the comparison of  $BrO$  shown in Figure 3h. We base our best estimate of PGI on a statistical analysis of both measurements, since we have no basis for assessing which observationally based estimate of  $Br_y$  is more likely to be correct. Finally, the fact that the CAM-chem-SD estimate for  $BrO$  shown in Figure 3h looks nearly identical compared to observations as the CAM-chem-SD estimate for  $Br_y$  shown in Figure 7d demonstrates that the representation of the  $BrO/Br_y$  ratio is comparable between our photochemical box model and the global model (Figure S9). Koenig et al. (2017) highlight large variations in the  $Br_y$  partitioning obtained with both box and global models in the upper troposphere, outside of the regions used here, particularly where aerosol SAD is below  $1 \times 10^{-8} \text{ cm}^2/\text{cm}^3$ . This suggests that further research regarding transport, recycling, and/or washout of inorganic bromine is still required.

Our estimate of PGI is based on inferred  $Br_y$  only within the stratosphere. As the GV aircraft travels deeper into the stratosphere, the  $BrO/Br_y$  ratio increases during both RF06 and RF15, due to the declines in atomic Br and HBr, driven by ambient  $O_3$  and heterogeneous processing. This behavior is consistent with the explanation for bromine partitioning described by Fernandez et al. (2014) and Koenig et al. (2017). Within the stratosphere, the contribution of  $BrONO_2$  to the  $Br_y$  budget increases as the mixing ratio of  $O_3$  exceeds 200 ppb (grey shaded portion of Figure 7b) and  $NO_2$  exceeds 50 ppt (Figure S2a). As discussed below,  $Br_y$  inferred for this flight segment is sensitive to the accuracy of the kinetic information used to define the rates of

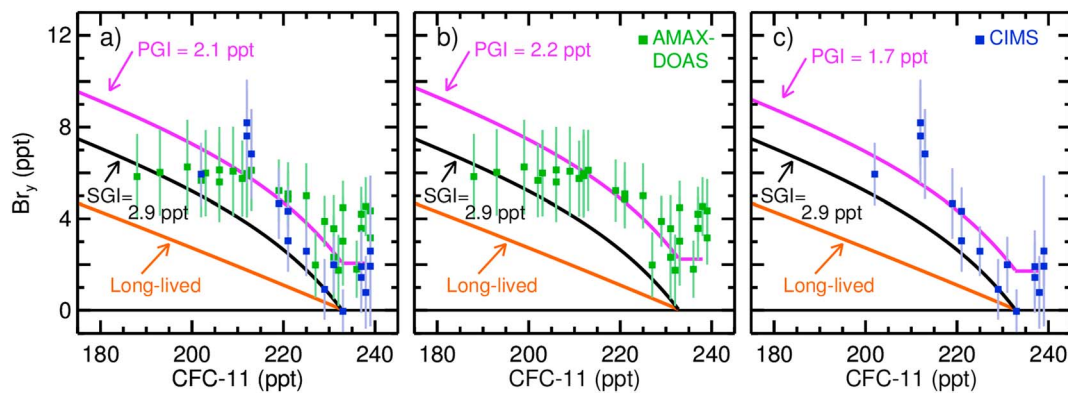


**Figure 8.** Stratospheric  $Br_y$  as a function of CFC-11 for winter 2014. In all panels, the square points are  $Br_y$  inferred from AMAX-DOAS (green) and CIMS (blue) measurements of BrO, averaged for 5 min centered at the time of AWAS measurements of CFC-11. The orange lines are  $Br_y^{SGI}$  for long-lived compounds, and the black lines show  $Br_y^{SGI}$  for the sum of long-lived and VLSL (dashed lines in Figure 6b). The purple lines are  $Br_y^{SGI} + PGI$ . (a) The mean and standard deviation of PGI estimated using both AMAX-DOAS and CIMS-inferred  $Br_y$  is  $2.1 \pm 1.3$  ppt. (b) PGI estimated using only AMAX-DOAS inferred  $Br_y$  is  $2.2 \pm 1.3$  ppt. (c) PGI estimated using only CIMS-inferred  $Br_y$  is  $1.7 \pm 1.3$  ppt.

formation and loss of  $BrONO_2$ , which currently has considerable uncertainty (Kreygy et al., 2013; Sioris et al., 2006). Most importantly, our estimate of PGI is weighted toward flight segments for which BrO constitutes about half of  $Br_y$ .

The relationship between the inferred  $Br_y$  and AWAS CFC-11 was used to estimate PGI (Figure 8). Five-minute averages of stratospheric  $Br_y$ , inferred from BrO observations, were calculated, centered at the time of each AWAS CFC-11 measurement. PGI was calculated from the mean difference between  $Br_y^{SGI}$  (black line in Figure 8) and inferred  $Br_y$ . The PGI estimate using both AMAX-DOAS and CIMS measurements is  $2.1 \pm 1.3$  ppt, where the reported uncertainty is the standard deviation of the mean (Figure 8a). PGI estimated using only AMAX-DOAS measurements is  $2.2 \pm 1.3$  ppt (Figure 8b) and using only CIMS measurements is  $1.7 \pm 1.3$  ppt (Figure 8c).

The overall PGI estimate was determined to be  $2.1 \pm 2.1$  ppt. The total uncertainty is the root sum of square combination of four factors: (a) the standard deviation about the mean of the PGI estimate, (b) the  $1\sigma$  measurement uncertainty in BrO, (c) the impact of JPL 2015 kinetic  $1\sigma$  uncertainties on the BrO/ $Br_y$  ratio, and (d)  $1\sigma$  uncertainties in observations other than BrO used to constrain the box model (Table S2). Of these factors, the largest contributions to the overall uncertainty in PGI (2.1 ppt) are the uncertainties in measured BrO (error bars in Figure 3g and 3h) and the standard deviation of the mean difference between inferred  $Br_y$  and  $Br_y^{SGI}$  (reported in the previous paragraph), which both happen to be equal to 1.3 ppt. The impact of chemical kinetics on our estimate of PGI is  $\sim 0.8$  ( $-0.67, +0.98$ ) ppt. The kinetic term is dominated by the JPL 2015 uncertainty in the rate constant of  $BrO + NO_2 + M$  (Text S3 and Figure S10a).

Ambient  $NO_2$  makes the smallest contribution to the uncertainty in PGI. In our base scenario, modeled  $NO_y$  is constrained by AMAX-DOAS measurements of  $NO_2$  (section 2.2). If modeled  $NO_y$  is instead constrained to chemiluminescence measurements of NO, the PGI estimate decreases by 0.6 ppt due to the use of lower mixing ratios of  $NO_2$  within the box model. Further details are provided in Text S3 and Figures S2a and S10b. Consequently, the lower limit of our PGI estimate includes the uncertainties introduced by constraining modeled  $NO_y$  to chemiluminescence NO.

Additionally, the analysis presented in this section and in section 3.1 was repeated using a dynamical definition of the tropopause (2 PVU, green lines in Figure 1) instead of the thermal tropopause. With the dynamical tropopause, the resulting  $SGI^{VLSL}$  increases to  $3.0 \pm 0.7$  ppt and the PGI decreases to  $1.7 \pm 2.0$  ppt, which is within the overall uncertainties calculated using the thermal tropopause.

Values of  $Br_y$  inferred from the AMAX-DOAS measurements of BrO level off, with respect to CFC-11, for mixing ratios of CFC-11 below about 210 ppt (green squares, Figure 8). This behavior is contrary to the theoretical expectation that  $Br_y$  should rise as CFC-11 declines. The lowest mixing ratios of CFC-11 are accompanied by sharp positive spikes in  $O_3$  (Figure 3d). As discussed in section 2.1.1, since the AMAX-DOAS instrument collects slant column measurements of BrO horizontally in front of the plane and in a narrow band above and



below the aircraft, it is possible that the sharp gradients in atmospheric composition, as observed by the in situ AWAS and chemiluminescence instruments, are not captured by the remote sensing AMAX-DOAS instrument. Conversely, since high levels of  $O_3$  can interfere with the CIMS measurements, sharp atmospheric gradients can also affect the in situ observations. Furthermore, for locations where peak  $O_3$  and  $NO_2$  are observed, the impact of kinetic uncertainties on  $BrONO_2$  kinetics increases. Consequently, we use the combination of the AMAX-DOAS and CIMS observations of  $BrO$  to calculate our reported values of  $Br_y^{VLS}$  and PGI. The  $2.1 \pm 2.1$  ppt PGI estimate presented here is in good agreement with previous ATTREX and CONTRAST studies. In the Navarro et al. (2015) analysis of ATTREX GWAS measurements, only CAM-chem-SD was used to estimate PGI. In their study, output from the CAM-chem-SD model at 17 km was used to estimate a value for PGI of  $1.97 \pm 0.21$  ppt. Our observational based estimate is nearly identical, albeit with larger uncertainty, which most probably arises because we consider a wider age-spectrum of air masses within the lower stratosphere. The two previous studies that analyzed CONTRAST measurements of  $BrO$  restricted their estimates of PGI to analysis of data collected in the upper troposphere and the bottom of the stratosphere (i.e., where  $O_3 < 200$  ppb and the observed ratio of  $H_2O/O_3 < 0.1$  ppm/ppb). The PGI estimate presented in Koenig et al. (2017) is  $2.6 \pm 0.6$  ppt based on remotely sensed AMAX-DOAS measurements and is slightly higher than our estimate of  $2.2 \pm 1.3$  ppt (Figure 8b) based on analysis of all AMAX-DOAS data collected for altitudes above the thermal tropopause. Chen et al. (2016) estimated a PGI of approximately 2 ppt based on  $Br_y$  inferred from in situ CIMS observations of  $BrO$  acquired for air parcels where  $O_3$  is between 100 and 200 ppb, which is in agreement with the  $1.7 \pm 1.3$  ppt estimate (Figure 8c) presented here based on our analysis of all CIMS  $BrO$  acquired in the stratosphere. Our study is the first to present a single estimate for PGI by combining measurements of  $BrO$  obtained by both the AMAX-DOAS and CIMS instruments during CONTRAST.

### 3.3. Stratospheric Bromine From VLS ( $Br_y^{VLS}$ )

The total contribution of VLS to stratospheric bromine is found by combining our  $SGI^{VLS}$  ( $2.9 \pm 0.6$  ppt) and PGI ( $2.1 \pm 2.1$  ppt) estimates, yielding  $5.0 \pm 2.1$  ppt of  $Br_y^{VLS}$ . The uncertainties in the  $SGI^{VLS}$  and PGI estimates are not additive, since our method implies that a decrease in  $SGI^{VLS}$  would cause a corresponding increase in PGI. Overall uncertainty in  $Br_y^{VLS}$  is dominated by the uncertainty in our estimate of PGI. The smaller range of values for PGI and  $Br_y^{VLS}$  are true if (a) the lower limits of the uncertainties in measurements of  $BrO$  are more accurate, (b) the kinetics governing the formation of  $BrONO_2$  are faster than the JPL 2015 recommendation, and/or (c) nitrogen oxide loading is better represented by chemiluminescence NO than by AMAX-DOAS  $NO_2$ . Conversely, the larger values of PGI and  $Br_y^{VLS}$  are true if (a) the upper limits of the uncertainties in measurements of  $BrO$  are more accurate, (b) the kinetics governing the formation of  $BrONO_2$  are slower than the JPL 2015 recommendation, and/or (c) nitrogen oxide loading is better represented by AMAX-DOAS  $NO_2$  than by chemiluminescence NO.

Our best estimate of  $Br_y^{VLS}$  of 5.0 ppt is in perfect agreement with the value given by WMO 2014. However, our  $\pm 2.1$  ppt uncertainty is smaller than the WMO 2014 uncertainty of  $\pm 3$  ppt. We also estimate that 58% of  $Br_y^{VLS}$  enters the stratosphere as organic compounds ( $SGI^{VLS} = 2.9 \pm 0.6$  ppt) and the remaining 42% enters as inorganic bromine (PGI =  $2.1 \pm 2.1$  ppt). In WMO 2014, the best estimate for  $SGI^{VLS}$  is 0.7 to 3.4 ppt based on observations of brominated VLS at the tropical tropopause, and the best estimate for PGI is 1.1 to 4.3 ppt based on modeling studies (Table 1–9 of Carpenter et al., 2014). In addition to observed  $SGI^{VLS}$  and modeled PGI, estimates of  $Br_y^{VLS}$  in WMO 2014 have been based on analysis of  $BrO$  profiles in the middle to upper stratosphere obtained by either ground-based (e.g., Schofield et al., 2004; Theys et al., 2007), balloon-borne (e.g., Dorf et al., 2008; Stachnik et al., 2013), or satellite instruments (e.g., Dorf et al., 2006; Kovalenko et al., 2007; McLinden et al., 2010; Parrella et al., 2013; Sioris et al., 2006). The mean value of the best estimate for  $Br_y^{VLS}$  from these studies is 6 ppt, with a range of 3 to 8 ppt (Carpenter et al., 2014). If the modification to the kinetics that govern the  $BrONO_2$  to  $Br_y$  ratio put forth by Kreygy et al. (2013) based on atmospheric observations is adopted, these values fall to a best estimate of 5 ppt, with a range of 2 to 8 ppt. This proposed kinetic revision would decrease our  $Br_y^{VLS}$  estimate by 0.5 ppt and is considered in our overall uncertainty (Text S3).

Also, our estimate is in close agreement with the  $5.2 \pm 2.5$  ppt value for  $Br_y^{VLS}$  given by Dorf et al. (2008) based on analysis of balloon-borne observations acquired at Teresina, Brazil ( $5.1^\circ S$ ,  $42.9^\circ W$ ) during June 2005. Dorf et al. (2008) estimated that a larger portion of the stratospheric transport of VLS occurred as

inorganic bromine ( $\text{PGI} = 4.0 \pm 2.5$  ppt) than found in our study. They also ascribed the same uncertainty to both  $\text{Br}_y^{\text{VLS}}$  and  $\text{PGI}$  (i.e.,  $\pm 2.5$  ppt), since organic bromine species are able to be measured with much better accuracy and precision than can be achieved for  $\text{BrO}$ . The need to infer total inorganic bromine from measured  $\text{BrO}$  adds an additional, important source of uncertainty (e.g., Kreygy et al., 2013) to estimates of both  $\text{PGI}$  and  $\text{Br}_y^{\text{VLS}}$ .

## 4. Comparison to CCMI Models

### 4.1. Model Descriptions

Output from 14 global models involved in CCMI (Eyring et al., 2013; Morgenstern et al., 2017) was analyzed to assess the representation of the stratospheric supply of bromine from VLS (Table 4). Thirteen of these models are chemistry-climate models (CCMs) that rely on internal, model generated transport fields, whereas TOMCAT is a chemical transport model (CTM) that uses fields from European Centre for Medium-Range Weather Forecasts reanalysis (ERA)-Interim meteorology (Dee et al., 2011). Three simulations of the EMAC CCM were considered. The EMAC-L47MA and EMAC-L90MA simulations use internally generated meteorological fields with 47 and 90 hybrid-pressure levels, respectively. The EMAC-L90MA-SD simulation (i.e., with 90 hybrid-pressure levels), nudged by Newtonian relaxation toward ERA-Interim meteorology (Dee et al., 2011), was examined to assess the effect of observed versus internally generated meteorology on the results of this study. The inclusion of EMAC in the multimodel mean analysis is based on the average of the three simulations, before combining with other models, so that EMAC does not have undue influence on the resulting multimodel mean.

For the CCMs considered in this study we have used monthly, zonal mean output of organic and inorganic bromine compounds as well as CFC-11 and tropopause pressure for January through March 2014 from the Ref-C2 scenario. These variables have been archived by the CCMI project and are maintained either by the National Center for Atmospheric Research Earth System Grid (CESM1-CAM4Chem and WACCM) or the British Atmospheric Data Centre (all other CCMs). The EMAC-L90MA-SD and TOMCAT CTM variables are zonally resolved, monthly mean output. The Ref-C2 simulations utilize the surface mixing ratios of ozone depleting substances given by the A1 scenario from the 2010 WMO Ozone Assessment (Montzka et al., 2011). Morgenstern et al. (2017) provides a high-level description of the global models involved in CCMI.

The CCMI models are grouped according to how they represent  $\text{Br}_y^{\text{VLS}}$ . As listed in Table 4, nine of the models provide an explicit simulation of at least the two major VLS ( $\text{CHBr}_3$  and  $\text{CH}_2\text{Br}_2$ ). The majority of the CCMs that explicitly represent VLS impose a 1.2 ppt surface mixing ratio for both  $\text{CH}_2\text{Br}_2$  and  $\text{CHBr}_3$ , as suggested by Eyring et al. (2013). The surface loading of VLS from Eyring et al. (2013) was designed to result in 4.5 to 5.0 ppt of  $\text{Br}_y^{\text{VLS}}$  since washout was expected to remove a fraction of the inorganic gases produced by oxidation of VLS in the troposphere. The EMAC model and TOMCAT CTM are exceptions among the explicit CCMI models for their treatment of  $\text{Br}_y^{\text{VLS}}$ . In addition to  $\text{CH}_2\text{Br}_2$  and  $\text{CHBr}_3$ , the EMAC simulations include bromine sources from sea-salt aerosols and three minor VLS ( $\text{CH}_2\text{BrCl}$ ,  $\text{CHBr}_2\text{Cl}$ , and  $\text{CHBrCl}_2$ ). Also, biogenic emissions of VLS in EMAC emissions are parameterized according to Warwick et al. (2006). Within TOMCAT the surface mixing ratios of  $\text{CHBr}_3$  and  $\text{CH}_2\text{Br}_2$  are each 1 ppt. Finally, the implementation of sources of VLS in the CESM1 CAM4-Chem version included in CCMI follows Eyring et al. (2013), while the CAM-chem-SD version used in section 2.1.2 to analyze CONTRAST and ATTREX observations relied on the Ordóñez et al. (2012) emission scenario.

The last five CCMs listed in Table 4 utilize a simplified treatment for VLS. Within these models, the surface mixing ratio of  $\text{CH}_3\text{Br}$  was increased by 5 ppt to represent the bromine loading from VLS. This surrogate method was described by Eyring et al. (2013) as an option for modeling groups that did not have the resources to add explicit treatment of VLS. The surface mixing ratio of  $\text{CH}_3\text{Br}$  was increased by 5 ppt since tropospheric loss of this compound, which is longer-lived than VLS, is expected to be small.

We have included all CCMI models that have archived model output for  $\text{CBr}_4$ ,  $\text{Br}_y$ , and CFC-11 for winter 2014. Except for the TOMCAT CTM and EMAC-L90MA-SD simulation, the model results are not based on observed transport fields and hence are not expected to match the actual meteorological conditions. However, due to changing anthropogenic emissions and regulation by the Montreal Protocol, the surface mixing ratios of  $\text{CH}_3\text{Br}$  and halons change over time. To assess the model representation of the bromine loading observed

**Table 4**  
The Bromine Sources Included in CCMI Models Considered by Our Study

Model	Bromine sources	References
ACCESS-CCM	CH <sub>3</sub> Br, CHBr <sub>3</sub> , CH <sub>2</sub> Br <sub>2</sub>	Stone et al. (2016)
CCSRNIES	CH <sub>3</sub> Br, halons, CHBr <sub>3</sub> , CH <sub>2</sub> Br <sub>2</sub>	Akiyoshi et al. (2016)
CESM1 CAM4- Chem	CH <sub>3</sub> Br, halons, CHBr <sub>3</sub> , CH <sub>2</sub> Br <sub>2</sub>	Lamarque et al. (2012); Tilmes et al. (2016)
CESM1 WACCM	CH <sub>3</sub> Br, halons, CHBr <sub>3</sub> , CH <sub>2</sub> Br <sub>2</sub>	Garcia et al. (2017); Marsh et al. (2013); Solomon et al. (2015)
CMAM	CH <sub>3</sub> Br, CHBr <sub>3</sub> , CH <sub>2</sub> Br <sub>2</sub>	Scinocca et al. (2008)
EMAC	CH <sub>3</sub> Br, halons, CHBr <sub>3</sub> , CH <sub>2</sub> Br <sub>2</sub> , minor VSLS, sea salt	Jöckel et al. (2016); Kerkweg et al. (2008)
NIWA-UKCA	CH <sub>3</sub> Br, CHBr <sub>3</sub> , CH <sub>2</sub> Br <sub>2</sub>	Morgenstern et al. (2009)
SOCOL3	CH <sub>3</sub> Br, halons, CHBr <sub>3</sub> , CH <sub>2</sub> Br <sub>2</sub>	Stenke et al. (2013)
TOMCAT CTM	CH <sub>3</sub> Br, halons, CHBr <sub>3</sub> , CH <sub>2</sub> Br <sub>2</sub>	Chipperfield (2006)
CNRM-CM5.3	CH <sub>3</sub> Br (+5 ppt), halons	Michou et al. (2011); Voldoire et al. (2012)
GEOSCCM	CH <sub>3</sub> Br (+5 ppt), halons	Oman et al. (2013)
MRI-ESM1	CH <sub>3</sub> Br (+5 ppt), halons	Deushi and Shibata (2011); Yukimoto et al. (2012)
ULAQ-CCM	CH <sub>3</sub> Br (+5 ppt), halons	Pitari et al. (2014)
UMSLIMCAT	CH <sub>3</sub> Br (+5 ppt), halons	Tian and Chipperfield (2005)

during the CONTRAST and ATTREX campaigns, output from all of the CCMI models was analyzed only for the time period January to March 2014.

#### 4.2. Multimodel Means

The goal of CCMI is to evaluate and improve the behavior of global models that have been designed to assess the interactions between climate change and atmospheric chemistry (Eyring et al., 2013; Morgenstern et al., 2017). Many scientific studies that utilize CCMI models have focused on stratospheric ozone (e.g., Fernandez et al., 2017; Oman et al., 2016; Sinnhuber & Meul, 2015). Since realistic representation of bromine is necessary to properly simulate stratospheric ozone, we compare the bromine loading in 14 CCMI models (Table 4) to the empirical estimate based on CONTRAST and ATTREX observations. Each CCMI model is classified as either having “explicit” or “surrogate” treatment of VSLS, as discussed in section 4.1.

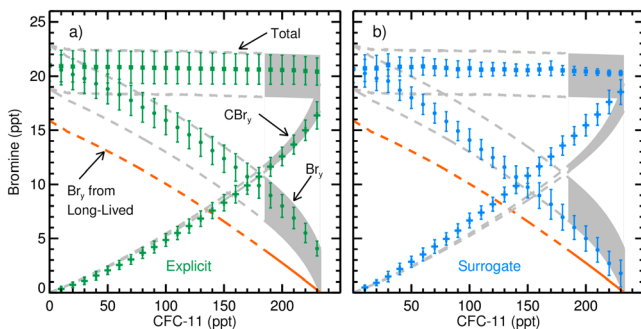


**Figure 9.** Observed and modeled relations of bromine as a function of CFC-11 for winter 2014. Observed relations of CBr<sub>y</sub>, Br<sub>y</sub>, and total bromine as a function of CFC-11 are shown in grey. The orange lines represent the expected rise of Br<sub>y</sub> from the stratospheric supply of long-lived compounds only. The shaded grey regions represent the range of uncertainty in the observed relation, and the dashed grey lines represent extrapolations of the upper and lower limits of the observed relations beyond the range of measured CFC-11. The observed CBr<sub>y</sub> relation includes  $2.9 \pm 0.6$  ppt from SGI<sup>VLSL</sup>, and the limits of this relation are defined according to the uncertainty in the linear fit of equation (2). The limits of both observed Br<sub>y</sub> and total bromine relations are defined according to the 0.0 to 4.2 ppt range in observed PGI. The points and error bars are the multimodel mean and standard deviation of CCMI models with (a) explicit and (b) surrogate representations of VSLS. Model output is for January to March 2014, filtered for poleward of 30°N and binned for every 10 ppt of CFC-11.

Multimodel means of bromine as a function of CFC-11 from explicit and surrogate models are shown in Figure 9. The modeled CBr<sub>y</sub>, Br<sub>y</sub>, and total bromine (CBr<sub>y</sub> + Br<sub>y</sub>) have been averaged within 10 ppt bins of modeled CFC-11. To properly compare observed and modeled bromine using CFC-11, model output for CFC-11 is scaled by the ratio of observed to modeled CFC-11 at the tropical tropopause (Table S4). Since the variation of CBr<sub>y</sub> compounds with CFC-11 is expected to be different in the tropics than in the extratropics (Volk et al., 1996), and the majority of the observations used in our study were obtained in the northern extratropics, model output was filtered to include output poleward of 30°N and between the model tropopause pressure and 1 hPa. Similar figures for all individual explicit and surrogate models are discussed in section 4.3.

The three observed bromine relations (total, organic decay, and inorganic rise) are shown in grey as functions of CFC-11 in Figure 9. The solid grey regions represent the observed range of CFC-11. The observed CBr<sub>y</sub> relation is based on the solid black line shown in Figure 6b. The observed Br<sub>y</sub> relation is inorganic bromine that forms upon stratospheric decay of all CBr<sub>y</sub> compounds (equation (4), lower limit of grey shading) plus the amount of inorganic product gas that is transported across the tropopause (PGI =  $2.1 \pm 2.1$  ppt, upper limit of grey shading). The lower and upper boundaries for Br<sub>y</sub> and for total bromine, which is the sum of observed CBr<sub>y</sub> and Br<sub>y</sub>, are both defined

**Table 5**  
Stratospheric Supply of Bromine for Winter 2014 From Observations and CCMI Models

Source	SGL <sup>LL</sup> (ppt)	SGL <sup>VLSL</sup> (ppt)	PGI (ppt)	Total (ppt)
<b>Observed</b>	<b>15.0 ± 0.2</b>	<b>2.9 ± 0.6</b>	<b>2.1 ± 2.1</b>	<b>20.0 ± 2.1</b>
ACCESS-CCM	13.7 ± 0.2	2.0 ± 0.1	3.7 ± 0.3	19.4 ± 0.05
CCSRNIES-MIROC3.2	12.9 ± 0.05	2.0 ± 0.05	4.4 ± 0.2	19.3 ± 0.03
CESM1 CAM4-chem	14.2 ± 0.2	2.2 ± 0.07	3.0 ± 0.4	19.3 ± 0.06
CESM1 WACCM	14.4 ± 0.2	2.3 ± 0.08	2.9 ± 0.4	19.6 ± 0.1
CMAM	14.0 ± 0.1	2.8 ± 0.09	3.1 ± 0.3	19.9 ± 0.02
EMAC-L47MA	12.9 ± 0.2	5.0 ± 0.3	4.8 ± 0.8	22.7 ± 0.5
EMAC-L90MA	13.1 ± 0.1	5.1 ± 0.2	4.6 ± 0.5	22.8 ± 0.5
EMAC-L90MA-SD	13.5 ± 0.2	5.7 ± 2.3	3.7 ± 0.8	22.9 ± 0.8
NIWA-UKCA	13.5 ± 0.1	1.9 ± 0.1	3.8 ± 0.3	19.2 ± 0.07
SOCOL3	14.4 ± 0.1	3.0 ± 0.2	5.3 ± 0.5	22.7 ± 0.02
TOMCAT CTM	14.6 ± 0.8	3.4 ± 0.9	2.3 ± 1.6	20.4 ± 0.02
<b>Explicit models</b>	<b>13.9 ± 0.6</b>	<b>2.8 ± 1.1</b>	<b>3.6 ± 0.9</b>	<b>20.3 ± 1.5</b>
CNRM-CM5.3	19.6 ± 0.1		0.9 ± 0.2	20.5 ± 0.01
GEOSCCM	19.5 ± 0.06		1.2 ± 0.2	20.7 ± 0.1
MRI-ESM1r1	19.4 ± 0.01		0.7 ± 0.01	20.0 ± 0.07
ULAQ-CCM	17.0 ± 0.2		1.3 ± 0.3	18.4 ± 0.2
UMSLIMCAT	19.6 ± 0.08		0.7 ± 0.1	20.3 ± 0.1
<b>Surrogate models</b>	<b>19.0 ± 1.1</b>		<b>1.0 ± 0.3</b>	<b>20.0 ± 1.0</b>

Note. Model entries are based on output at the tropical tropopause pressure for January to March 2014. Bold entries are based on observations and the multimodel mean of explicit and surrogate models.

according to the 0.0 to 4.2 ppt range estimated for PGI. For comparison, an additional orange line is shown in each panel to indicate the expected Br<sub>y</sub> relation due to supply from only halons and CH<sub>3</sub>Br (equation (4), orange dashed lines in Figure 6b). Since the lowest mixing ratio for CFC-11 observed during CONTRAST was 188 ppt, bromine relations at lower mixing ratios of CFC-11 are extrapolated and shown using dashed lines (only upper and lower limits are shown). These extrapolations are based on the values reported in Table 2 as well as equations (3) and (4), following an approach that is commonly used to relate aircraft observations to global model output (e.g., Wamsley et al., 1998).

Figure 9a shows results from the multimodel mean of CCMI models with explicit representation of VLSL. The values of CBr<sub>y</sub> and Br<sub>y</sub> in these models follow the observed curvature of the respective observed bromine versus CFC-11 relations quite well. However, the values of Br<sub>y</sub> tend to lie either close to the central values of our empirical estimate or along the upper limit of the range for all levels of CFC-11. The good agreement between the modeled and observed relations implies that mean SGL<sup>VLSL</sup> and PGI in explicit models are similar to that determined using CONTRAST and ATTREX data.

Table 5 compares the multimodel mean and standard deviation of SGI and PGI from the CCMI models to the same values inferred from the field observations. For this table, SGL<sup>LL</sup> and SGL<sup>VLSL</sup> were calculated respectively from the sum of long-lived bromocarbons and VLSL at the tropopause pressures, reported by the global models, within the tropics (20°S to 20°N). Likewise, PGI and total bromine were calculated from the mixing ratios of modeled Br<sub>y</sub> and the sum of modeled organic and inorganic bromine, respectively, at the tropical tropopause. Multimodel mean values are highlighted in bold and are calculated separately for explicit and surrogate models. Results for individual models are discussed in section 4.3.

The mean value of SGL<sup>VLSL</sup> for the explicit models is 2.8 ± 1.1 ppt, which is close to the observed value of 2.9 ± 0.6 ppt (Table 5). As described in section 4.1, the Eyring et al. (2013) emission scheme for VLSL in CCMI models prescribes a sum of 6 ppt of bromine from VLSL at the surface. This value is consistent with the 5.9 ± 0.5 ppt of bromine from VLSL observed between altitudes of 0 and 0.5 km in the TWP during CONTRAST (Figure 5). The mean value of SGL<sup>LL</sup> is 13.9 ± 0.6 ppt for explicit models, which is lower than the observed value of 15.0 ± 0.2 ppt. All CCMI models assign surface mixing ratios of CH<sub>3</sub>Br and halons according to the A1 scenario from the 2010 WMO Ozone Assessment, for a sum of 15.0 ppt of bromine. The WMO 2010 values for CH<sub>3</sub>Br and halons are all within 0.1 ppt of the mixing ratios given in the WMO 2014 scenario (black dashed lines in Figure S8) and within 0.2 ppt of surface CONTRAST observations in the TWP. Consequently, the lower value of SGL<sup>LL</sup> within explicit models indicates a higher tropospheric loss of long-lived bromocarbons in CCMI models than observed.

Finally, the mean value of PGI for explicit models is 3.6 ± 0.9 ppt. This value is larger than the observed value of 2.1 ± 2.1 ppt but within the observed range of uncertainty. As shown in section 4.3, all nine models with explicit treatment of VLSL estimate higher PGI than observed. This reflects the tendency of the modeled Br<sub>y</sub> to be along the upper range of observations in Figure 9a. The CCMI model representation of PGI depends on the rate of decomposition of organic bromocarbons in the tropical troposphere (e.g., Rex et al., 2014) and the subsequent efficiency of washout of inorganic product gases (e.g., Sinnhuber & Folkins, 2006). Additionally, the inclusion of both heterogeneous reactions of inorganic bromine species (e.g., Fernandez et al., 2014) and the sea-salt dehalogenation source (e.g., Schmidt et al., 2016; Wang et al., 2015) will also affect the representation of PGI within individual CCMI models. Finally, the faster decomposition of SGL<sup>LL</sup> within explicit models compared to observations, discussed above, could be a contributing factor to the overestimate of PGI. Further research is required to understand the role of these factors in driving the differences

of computed PGI shown in Table 5, as well as the tendency for all of the models to exceed our central empirical estimate of 2.1 ppt.

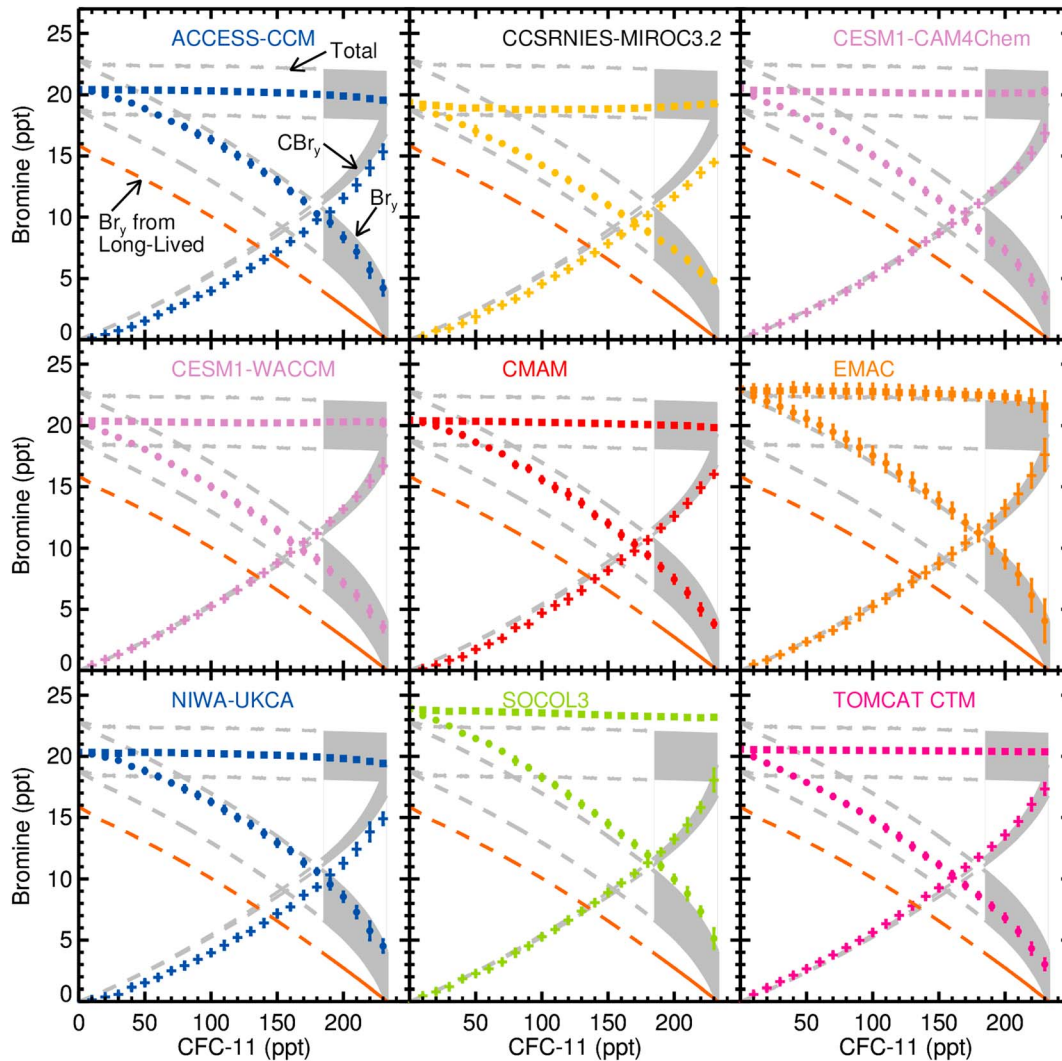
The bromine relations in CCMI models with surrogate VSLs are shown in Figure 9b. Since  $\text{CH}_3\text{Br}$  has a longer photochemical lifetime than VSLs in the lower stratosphere, the decay of  $\text{CBr}_y$  with decreasing mixing ratios of CFC-11 is slower in these models compared to both observations (Figure 9b) and  $\text{CBr}_y$  from models that use an explicit treatment (Figure 9a). Consequently,  $\text{Br}_y$  in the surrogate CCMI models most commonly lies along the lower limit of the empirical range of the  $\text{Br}_y$  versus CFC-11 relation, particularly in the lower stratosphere (i.e., for the highest mixing ratios of CFC-11). As a result, these models could underestimate the role of bromine in photochemical loss of ozone in this region of the atmosphere. For older air parcels (i.e., low mixing ratios of CFC-11),  $\text{Br}_y$  in the surrogate models resembles the observed  $\text{Br}_y$  versus CFC-11 relation quite well, due to the release of bromine contained in  $\text{CH}_3\text{Br}$ .

Table 5 lists numerical values only for  $\text{SGI}^{\text{LL}}$ , PGI, and total bromine from the surrogate models. The entry for  $\text{SGI}^{\text{LL}}$  in Table 5 represents SGI by all organic compounds, since VSLs are not explicitly simulated. These surrogate models exhibit a PGI of  $1.0 \pm 0.3$  ppt, which is lower than both the observed value of  $2.1 \pm 2.1$  ppt as well as that found by the explicit models,  $3.6 \pm 0.9$  ppt. This tendency is due to the relatively long tropospheric lifetime of  $\text{CH}_3\text{Br}$  compared to  $\text{CHBr}_3$  and demonstrates a potential shortcoming in the surrogate treatment of VSLs.

The mean total bromine loadings of  $20.3 \pm 1.5$  ppt in the explicit models as well as the  $20.0 \pm 1.0$  ppt in the surrogate models are both close to the  $20.0 \pm 2.1$  ppt observed value (Table 5). Furthermore, for more photochemically aged air (i.e., CFC-11 less than  $\sim 120$  ppt), the representation of  $\text{Br}_y$  in surrogate models is within the observed range (Figure 9b). Consequently, the representation of stratospheric bromine for studies of polar ozone should be reliable for both explicit and surrogate treatments of VSLs. All CCMI models that use either explicit or surrogate representations of VSLs lie much closer to the empirical estimate of  $\text{Br}_y$  (grey) than to the estimate using only  $\text{CH}_3\text{Br}$  and halons (orange). As a result, both CCMI methods for including VSLs are able to more closely simulate observed stratospheric bromine than would be found if VSLs had been completely neglected.

Our estimates for stratospheric bromine injection in Table 5 are calculated using the tropopause values throughout the tropics from the CCMI models. Because the output from the majority of the CCMs are only available as zonal means, we are not able to separate the contribution of the TWP. The precise values for SGI and PGI within the CCMs can depend on details of the meteorological fields. However, a comparison between EMAC simulations that used internally generated transport fields and that relied on observed meteorology revealed no discernible difference in the resulting bromine relations in the middle and upper stratosphere and a small difference, well within the observational uncertainty, for the LMS (Text S4 and Figure S11). Furthermore, values of SGI and PGI from the CCMI models calculated using the tracer-tracer relation approach are similar to those given in Table 5 (Table S5). The mean PGI for explicit models calculated using tracer-tracer relations is 0.6 ppt higher than the value given in Table 5. The difference between all other multimodel mean values in Tables 5 and S5 are between  $-0.2$  and  $0.3$  ppt. Within individual models, there is no clear pattern to these offsets.

Previous modeling studies have evaluated the ability of different emission inventories of VSLs to represent stratospheric bromine injection. Our estimates for  $\text{SGI}^{\text{VSLs}}$  of  $2.9 \pm 0.6$  ppt (observed) and  $2.8 \pm 1.1$  ppt (explicit CCMI models; Table 5) are slightly higher than the  $\text{SGI}^{\text{VSLs}}$  value of 2.0 ppt (range 1.2 to 2.5 ppt) reported by Hossaini et al. (2016). Additionally, the values of  $\text{Br}_y^{\text{VSLs}}$  calculated from the sum of PGI and  $\text{SGI}^{\text{VSLs}}$  are  $5.0 \pm 2.1$  ppt based on observations and  $6.4 \pm 1.4$  ppt in explicit models. Both values of  $\text{Br}_y^{\text{VSLs}}$  are well within the 4 to 8 ppt range reported by Hossaini et al. (2013). While the global models considered in the Hossaini et al. (2016) and Hossaini et al. (2013) studies use observation-based emission inventories for VSLs (Liang et al., 2014; Ordóñez et al., 2012; Ziska et al., 2013), the CCMI models (with the exception of EMAC) use a more simplified approach of prescribed surface mixing ratios of VSLs. It is therefore reassuring that this simplified approach is able to adequately represent stratospheric injection of VSLs. Explicit representation of oceanic emissions of VSLs provides an avenue for assessing the impact of climate change and oceanic biology on atmospheric bromine that is inaccessible upon use of prescribed mixing ratios (Falk et al., 2017; Lennartz et al., 2015). Our analysis of the aircraft observations in the TWP, such as the grey curves in Figure 9,



**Figure 10.** Same as Figure 9 but for individual CCMI models with explicit representations of VSLs (Table 4). The mean of three EMAC simulations, shown in Figure S11, is shown for EMAC.

provides a benchmark for evaluation of the simulated representation of stratospheric bromine within global models.

### 4.3. Individual Models

Figure 10 shows bromine relations from all individual CCMI models with explicit treatment of VSLs. Each panel was prepared in the same manner as Figure 9, and the panel for EMAC uses the mean of the three simulations shown in Figure S11. Three of the CCMI models with explicit representations of VSLs (ACCESS, CCSRNIIES, and NIWA-UKCA) have  $CBr_y$  mixing ratios that lie a few ppt below the observed relation. However, for all three of these models, total bromine lies within the observed range of uncertainty. Table 5 also includes  $SGI^{VSLs}$  values for each individual CCMI model. Of the CCMI models with explicit VSLs, values of  $SGI^{VSLs}$  in WACCM, CMAM, SOCOL3, and TOMCAT are within the observed  $2.9 \pm 0.6$  ppt range. Additionally, the values of  $SGI^{VSLs}$  in all three EMAC simulations are about 2 ppt above the observed central value. The tropical tropopause values of  $SGI^{VSLs}$  in the remaining four models with explicit treatment (ACCESS, CCSRNIIES, CAM4Chem, NIWA-UKCA) are 0.7 to 1 ppt below the observed central value. All explicit models, except EMAC and TOMCAT, follow the same boundary conditions for VSLs from the Eyring et al. (2013) emission scheme. Consequently, the differences in  $SGI^{VSLs}$  between these models are due to model variations in the convective lofting and chemical removal (i.e., reaction with OH and loss by photolysis) of these compounds in the tropical troposphere.

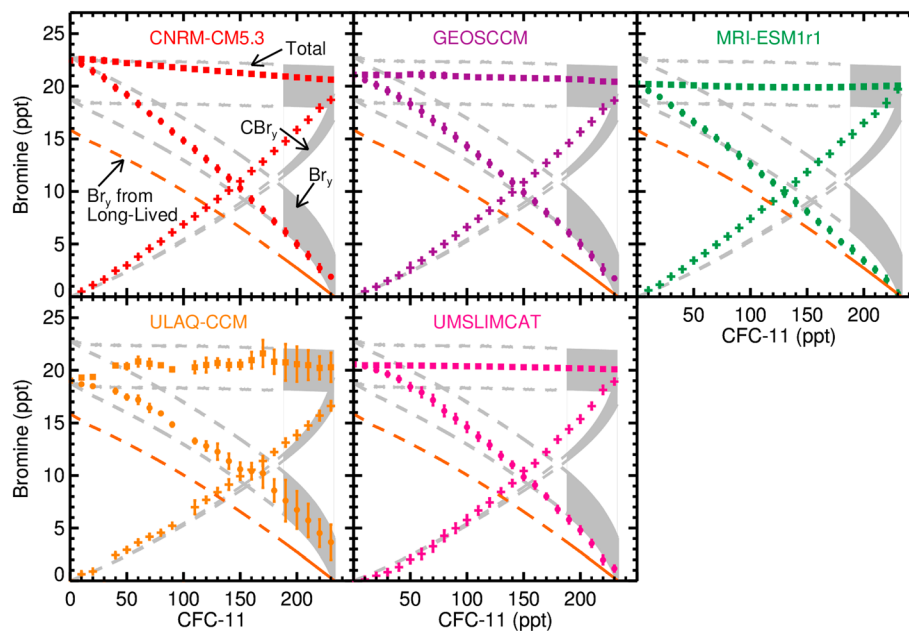


**Figure 11.** Same as Figure 9 but for individual CCMI models with surrogate representations of VSL (Table 4).

The EMAC simulations rely on geographical oceanic emission fields for  $\text{CHBr}_3$ ,  $\text{CH}_2\text{Br}_2$ , and minor VSLs from Warwick et al. (2006). As a result, offsets between  $\text{SGI}^{\text{VSL}}$  from the EMAC simulations and the other CCMI models are at least partially due to differences in how the tropospheric behaviors of the source gases are simulated. Mixing ratios of  $\text{CHBr}_3$  modeled using the Warwick et al. (2006) emissions have been shown to exceed observed values in Southeast Asia, which led to a suggested downward revision in the local rate of emission (Pyle et al., 2011). The observations considered by Pyle et al. (2011) were collected near the location sampled during CONTRAST and ATTREX. Therefore, the tendency for  $\text{CBr}_y$  from EMAC to lie above our observed value (Figure 10) will likely be resolved upon application of the downward revision in the emission of  $\text{CHBr}_3$ .

As discussed in section 4.2, the multimodel mean  $\text{Br}_y$  (Figure 9a) and PGI (Table 5) in explicit models are within the upper portion of the observed range. Similarly, in Figure 10 the values of  $\text{Br}_y$  from the explicit models tend to lie either close to the central values of our empirical estimate (CCSRNIES, CAM4Chem, WACCM, CMAM, and TOMCAT) or along the upper limit of the range (ACCESS, EMAC, NIWA-UKCA, and SOCOL3). CAM4Chem and WACCM both rely on the Community Earth System Model (CESM) framework, which we have also used to define the halon-1301 versus CFC-11 relation, because halon-1301 was not measured during CONTRAST and ATTREX. Since halon-1301 supplies 3.24 ppt to the bromine budget, this could contribute to the similarity between the results from these models and our estimated  $\text{Br}_y$  versus CFC-11 relation. Additionally,  $\text{CH}_3\text{Br}$  in ACCESS, CMAM, and NIWA-UKCA was scaled to represent halon loading (Stone et al., 2016). Since  $\text{CH}_3\text{Br}$  has a shorter photochemical lifetime than halons (Table 2), the use of  $\text{CH}_3\text{Br}$  to represent halons likely results in faster release of  $\text{Br}_y$  in these models, contributing to higher  $\text{Br}_y$  loading in the lower stratosphere.

The representations of PGI in CCSRNIES, SOCOL3, and all EMAC simulations are 0.4 to 1.3 ppt larger than the observed upper limit of 4 ppt (Table 5). As a result, the  $\text{Br}_y$  loadings in these models fall along the upper limit of the observed  $\text{Br}_y$  versus CFC-11 relation at the base of the stratosphere (i.e., where CFC-11 = 230 ppt in Figure 10). However, because  $\text{SGI}^{\text{LL}}$  and  $\text{SGI}^{\text{VSL}}$  are both low in CCSRNIES compared to other models as well as observations, inorganic bromine loading in CCSRNIES agrees well with observations. The higher value of PGI in EMAC is due to the use of emission fields from Warwick et al. (2006), as explained above for the discussion of  $\text{SGI}^{\text{VSL}}$ . The SOCOL3 simulation has the largest value of PGI ( $5.3 \pm 0.5$  ppt), which lies above the observed upper limit of 4 ppt. For SOCOL3 and EMAC, the  $\text{Br}_y$  versus CFC-11 relations lie at or just above the upper range of our uncertainty.

The bromine relations in individual surrogate models are shown in Figure 11. Comparisons between these models and the observed bromine relations are consistent with the discussion provided in section 4.2. Furthermore, the total bromine loading in four of the surrogate models (CNRM-CM5.3, GEOSCCM, MRI, and UMSLIMCAT), given in the last column of Table 5, is close to the  $20.0 \pm 2.1$  ppt estimate based on CONTRAST and ATTREX observations. For these four models, the representation of stratospheric bromine for studies of polar ozone should be reliable. Based on the mean mixing ratio at the tropical tropopause, the total bromine loading in ULAQ is  $18.4 \pm 0.2$  ppt, which is at the lower limit of the range of uncertainty. However, within the stratosphere, total bromine loading in ULAQ exhibits scatter around 20 ppt (orange squares in Figure 11), which is much closer to the observed best estimate. Furthermore, PGI and total bromine loading in ULAQ calculated using the tracer-tracer relation method are about 2 ppt larger than found using model output at the tropical tropopause (Table S5). This discrepancy between the two approaches for estimating stratospheric injection of bromine is unique to ULAQ and is presently not understood.

## 5. Conclusions

The combined organic and inorganic bromine measurements collected during the CONTRAST and ATTREX aircraft campaigns in the TWP during winter 2014 provide a unique opportunity to study the contribution of VSLS to stratospheric bromine. The TWP is a region of strong convection and is the dominant pathway for short-lived compounds to reach the stratosphere, particularly during boreal winter. The payloads onboard the CONTRAST and ATTREX aircrafts included instruments that measured BrO, a suite of long-lived bromocarbons, VSLS, many other chemical constituents critical to our analysis (i.e., O<sub>3</sub>, NO, NO<sub>2</sub>, CFC-11, H<sub>2</sub>O, CO, and CH<sub>4</sub>), as well as spectral actinic flux and aerosol SAD. Data from the CONTRAST and ATTREX campaigns provide the first opportunity to quantify the gas phase bromine budget, across the TTL and extending into the LMS of the critically important TWP, in a comprehensive manner that includes direct observations of organic and inorganic bromine species.

Empirical relations between bromocarbons and CFC-11, a tracer of photochemical aging across the tropopause, were developed using WAS measurements. These bromocarbon-tracer relations were used to quantify the stratospheric injection of long-lived substances and VSLS in organic form (SGI). Based on this analysis, the contribution to stratospheric bromine from VSLS (SGI<sup>VSLS</sup>) was determined to be  $2.9 \pm 0.6$  ppt. This estimate is slightly lower than the  $3.4 \pm 0.3$  ppt bromine content of organic VSLS observed at the average cold-point tropopause height (17 km) in the TWP during ATTREX. Estimates for SGI<sup>VSLS</sup> found by both methods exceed the WMO 2014 best estimate of 1.4 ppt but lie within their upper uncertainty range (0.7 to 3.4 ppt), which was based on prior observations near the tropical tropopause (Carpenter et al., 2014). The ATTREX value of  $3.4 \pm 0.3$  ppt is likely influenced by vigorous convection during boreal winter in the TWP, and therefore could be biased high relative to the tropical average SGI<sup>VSLS</sup>. We give  $2.9 \pm 0.6$  ppt as our best estimate for SGI<sup>VSLS</sup> because this value, found using the tracer-based approach, is based on analysis of data collected in the stratosphere that incorporates air masses with a wide range of convective histories throughout the tropics. Further research is needed to define possible seasonal and interannual variability in SGI<sup>VSLS</sup> (e.g., Fiehn et al., 2018; Hossaini et al., 2016).

Two flights during CONTRAST sampled the extratropical stratosphere by crossing the subtropical jet off the coast of Japan. Observations of BrO obtained during these flights by two instruments, AMAX-DOAS (Koenig et al., 2017) and CIMS (Chen et al., 2016), were combined with a photochemical box model to yield estimates of gas phase Br<sub>y</sub>. This empirical estimate of Br<sub>y</sub> was combined with observations of long-lived bromocarbons and VSLS to estimate the stratospheric injection of bromine that crosses the tropopause in inorganic form (PGI). Our best estimate of PGI is  $2.1 \pm 2.1$  ppt. The use of empirical bromocarbon-tracer relations builds on previous CONTRAST and ATTREX studies by providing a method for estimating PGI that considers the stratospheric decay of source gases and is applied to a large ensemble of stratospheric air masses. In the TWP, PGI represents both the decomposition products of brominated VSLS and the transport of labile inorganic species produced by brominated sea salt throughout the troposphere. Our value is within the 1.1 to 4.3 ppt range for PGI given by WMO 2014, which was largely based on model estimates of the whole tropical region. The largest contributor to the overall uncertainty in our estimate of PGI is the measurement uncertainty of BrO. Additionally, observations of BrO from both instruments exhibit considerable deviation about the respective means, which also contributes to the



### Acknowledgments

We sincerely appreciate the helpful comments from three anonymous reviewers that have led to a substantial improvement in the paper. The CONTRAST field deployment was supported by the U.S. NSF, and the ATTREX field deployment was supported by the National Aeronautics and Space Administration (NASA). We greatly appreciate the support of pilots, meteorological forecasters, flight planners, and a wide range of logistical support that enabled the acquisition of the observations. P. A. W., R. J. S., T. P. C., J. M. N., and D. C. A. received support from NSF, NASA Atmospheric Composition Modeling and Analysis Program (ACMAP), and the NASA Modeling, Analysis, and Prediction (MAP). D. C. A. also received support from the NASA Upper Atmospheric Research Program. J. M. N. was also supported by the NASA Postdoctoral Program at the NASA Goddard Space Flight Center, administered by Universities Space Research Association under contract with NASA. R. V. acknowledges funding from NSF awards AGS-1261740 and AGS-1620530. CONTRAST data are publicly available at "[http://data.eol.ucar.edu/master\\_list/?project=CONTRAST](http://data.eol.ucar.edu/master_list/?project=CONTRAST)." ATTREX data are publicly available at "<https://espoarchive.nasa.gov/archive/browse/attrex/id4/GHawk>." The National Center for Environmental Prediction (NCEP) meteorological data are available at "<https://doi.org/10.5065/D6M043C6>." CCM1 outputs from CESM1-WACCM and CESM1-CAM4Chem are archived by the National Center for Atmospheric Research (NCAR) at "[www.earthsystem-grid.org](http://www.earthsystem-grid.org)," and NCAR is sponsored by NSF. CCM1 output from the EMAC-L90MA-SD simulation is available at "<https://doi.org/10.5281/zenodo.1204495>." All other CCM1 simulations are archived by the British Atmospheric Data Centre at "<http://badc.nerc.ac.uk/>". Output from CAM-chem-SD is available as "NCAR/ACD CAMChem 1 Degree Forecast" at "[http://catalog.eol.ucar.edu/contrast/model/CAMChem\\_NCAR\\_1deg/](http://catalog.eol.ucar.edu/contrast/model/CAMChem_NCAR_1deg/)". WACCM and CAM-Chem are components of the Community Earth System Model (CESM), which is also supported by NSF. Computing resources were provided by NCAR's Climate Simulation Laboratory, sponsored by NSF and other agencies. This research was enabled by the computational and storage resources of NCAR's Computational and Information System Laboratory (CISL). R. S. and K. A. S., with ACCESS-CCM, acknowledge support from Australian Research Council's Centre of Excellence for Climate System Science (CE110001028),

overall uncertainty in PGI. The chemical kinetics that drive the ratio of BrO to Br<sub>y</sub> as well as ambient NO<sub>2</sub> and NO also contribute to the 2.1 ppt total uncertainty in PGI.

Our best estimate for the total contribution of VSLs to stratospheric bromine (Br<sub>y</sub><sup>VSLs</sup>) is 5.0 ± 2.1 ppt. This estimate agrees with the 5 ± 3 ppt assessed value given in WMO 2014, albeit with lower uncertainty. Our overall uncertainty in Br<sub>y</sub><sup>VSLs</sup> is dominated by the contribution of PGI, which in turn depends on the uncertainty in measured BrO. The value for Br<sub>y</sub><sup>VSLs</sup> given in WMO 2014 is mainly based on model estimates of BrO near the tropical tropopause as well as stratospheric slant column measurements of BrO. There are large uncertainties in calculating BrO near the tropical tropopause due to aerosol uptake and washout (e.g., Sinnhuber & Folkins, 2006), spatial distribution of biogenic emissions of VSLs (e.g., Hossaini et al., 2013), the strength of convection (e.g., Fernandez et al., 2014), the efficiency of removal of VSLs by OH (e.g., Rex et al., 2014), and the production of labile bromine from sea-salt aerosol (e.g., Schmidt et al., 2016). Given these uncertainties, an empirically based estimate for PGI based on measured BrO in the Western Pacific constitutes a significant step forward in our understanding of the effect of oceanic biology on stratospheric composition.

Our best estimate of Br<sub>y</sub><sup>VSLs</sup> of 5.0 ppt is the same as the WMO 2014 value. However, we apportion a larger fraction of the stratospheric transport of VSLs to source gases, 2.9 ppt versus the WMO 2014 value of 1.4 ppt based on prior observations at 17 km in the tropics. The consistency of our two estimates of SG1<sup>VSLs</sup> further supports the notion that cross tropopause transport of brominated very short-lived source gases is higher than given in the WMO 2014 assessment. Prior estimates of SG1<sup>VSLs</sup> have focused on analysis of data collected in the upper tropical troposphere at specific locations, outside of the TWP. Our best estimate is based on the use of tracer-based analysis of air masses sampled in the extratropical lower stratosphere, which reflects the influence of diverse convective histories throughout the tropics. Our estimate of SG1<sup>VSLs</sup> emphasizes the importance of including measurements from convectively active regions in the recommended values of SG1<sup>VSLs</sup> and PGI. Further research is required to quantify the temporal variability in Br<sub>y</sub><sup>VSLs</sup>, as well as possible spatial and time-dependent variations in the relative contributions of SG1<sup>VSLs</sup> and PGI (e.g., Fiehn et al., 2018; Hossaini et al., 2016).

We have also provided a comprehensive comparison to the representation of brominated VSLs within 14 global models that participated in CCMI (Morgenstern et al., 2017). The CCMI models that have explicit treatment of VSLs simulate SG1<sup>VSLs</sup> in a manner that is in very good agreement with observations. These models also represent PGI that is either close to our best empirical estimate or near the upper range of the observed uncertainty. Conversely, CCMI models that have surrogate treatment of VSLs (i.e., longer-lived CH<sub>3</sub>Br is used as a proxy for VSLs) simulate stratospheric injection of Br<sub>y</sub> that is close to the lower range of our observationally constrained estimate. The difference between explicit and surrogate treatment of VSLs is driven by slower decay of CH<sub>3</sub>Br relative to VSLs.

The representation of total stratospheric bromine within CCMI models is significantly improved upon consideration of either treatment of VSLs. The multimodel mean of total bromine within explicit and surrogate models is 20.3 ± 1.5 ppt and 20.0 ± 1.0 ppt, respectively, in excellent agreement with the 20.0 ± 2.1 ppt expected based on our observations. Methyl bromide and halons, long-lived sources, provided about 15 ppt of total bromine to the stratosphere in winter 2014. Therefore, either representation of VSLs provides a demonstrable, significant improvement over previous versions of these models that neglected the effect of VSLs on stratospheric bromine. The current formulation of bromine within the CCMI models should therefore provide more reliable simulations of the recovery of the Antarctic ozone hole (Fernandez et al., 2017; Oman et al., 2016), the effect of volcanic activity on midlatitude ozone (Feng et al., 2007; Klobas et al., 2017; Salawitch et al., 2005), the impact of geoengineering of climate on ozone (Tilmes et al., 2012, 2008), and tropospheric residual BrO inferred from satellite observations (Choi et al., 2012; Salawitch et al., 2010; Theys et al., 2011) compared to coupled chemistry-climate simulations that supply stratospheric bromine from only CH<sub>3</sub>Br and halons.

### References

- Akiyoshi, H., Nakamura, T., Miyasaka, T., Shiotani, M., & Suzuki, M. (2016). A nudged chemistry-climate model simulation of chemical constituent distribution at northern high-latitude stratosphere observed by SMILES and MLS during the 2009/2010 stratospheric sudden warming. *Journal of Geophysical Research: Atmospheres*, 121, 1361–1380. <https://doi.org/10.1002/2015JD023334>

the Australian Government's National Computational Merit Allocation Scheme (q90), and Australian Antarctic science grant program (FoRCES 4012). CCSRNIES research was supported by the Environment Research and Technology Development Fund (2-1303 and 2-1709) of the Ministry of the Environment, Japan, and computations were performed on NEC-SX9/A(ECO) computers at the CGER, NIES. The EMAC simulations have been performed at the German Climate Computing Centre (DKRZ) through support from the Bundesministerium für Bildung und Forschung (BMBF). DKRZ and its scientific steering committee are gratefully acknowledged for providing the HPC and data archiving resources for the consortial project ESCiMo (Earth System Chemistry integrated Modelling). The TOMCAT modeling was supported by NERC NCAS and the SISLAC project (NE/R001782/1), and the simulations were performed on the Archer and Leeds HPC Systems.

- Anderson, D. C., Nicely, J. M., Salawitch, R. J., Canty, T. P., Dickerson, R. R., Hanisco, T. F., et al. (2016). A pervasive role for biomass burning in tropical high ozone/low water structures. *Nature Communications*, 7(10267). <https://doi.org/10.1038/ncomms10267>
- Andrews, S. J., Carpenter, L. J., Apel, E. C., Atlas, E., Donets, V., Hopkins, J. R., et al. (2016). A comparison of very short lived halocarbon (VLSL) and DMS aircraft measurements in the tropical West Pacific from CAST, ATTREX and CONTRAST. *Atmospheric Measurement Techniques*, 9(10), 5213–5225. <https://doi.org/10.5194/amt-9-5213-2016>
- Aschmann, J., & Sinnhuber, B. M. (2013). Contribution of very short-lived substances to stratospheric bromine loading: Uncertainties and constraints. *Atmospheric Chemistry and Physics*, 13(3), 1203–1219. <https://doi.org/10.5194/acp-13-1203-2013>
- Aschmann, J., Sinnhuber, B. M., Atlas, E. L., & Schauffler, S. M. (2009). Modeling the transport of very short-lived substances into the tropical upper troposphere and lower stratosphere. *Atmospheric Chemistry and Physics*, 9(23), 9237–9247. <https://doi.org/10.5194/acp-9-9237-2009>
- Aschmann, J., Sinnhuber, B. M., Chipperfield, M. P., & Hossaini, R. (2011). Impact of deep convection and dehydration on bromine loading in the upper troposphere and lower stratosphere. *Atmospheric Chemistry and Physics*, 11(6), 2671–2687. <https://doi.org/10.5194/acp-11-2671-2011>
- Avallone, L. M., & Prather, M. J. (1997). Tracer-tracer correlations: Three-dimensional model simulations and comparisons to observations. *Journal of Geophysical Research*, 102(D15), 19,233–19,246. <https://doi.org/10.1029/97JD01123>
- Baidar, S., Oetjen, H., Coburn, S., Dix, B., Ortega, I., Sinreich, R., & Volkamer, R. (2013). The CU Airborne MAX-DOAS instrument: Vertical profiling of aerosol extinction and trace gases. *Atmospheric Measurement Techniques*, 6(3), 719–739. <https://doi.org/10.5194/amt-6-719-2013>
- Bergman, J. W., Jensen, E. J., Pfister, L., & Yang, Q. (2012). Seasonal differences of vertical-transport efficiency in the tropical tropopause layer: On the interplay between tropical deep convection, large-scale vertical ascent, and horizontal circulations. *Journal of Geophysical Research*, 117, D05302. <https://doi.org/10.1029/2011JD016992>
- Brinckmann, S., Engel, A., Bönisch, H., Quack, B., & Atlas, E. (2012). Short-lived brominated hydrocarbons—Observations in the source regions and the tropical tropopause layer. *Atmospheric Chemistry and Physics*, 12(3), 1213–1228. <https://doi.org/10.5194/acp-12-1213-2012>
- Burkholder, J. B., Sander, S. P., Abbatt, J., Barker, J. R., Huie, R. E., Kolb, C. E., et al. (2015). *Chemical kinetics and photochemical data for use in atmospheric studies, evaluation number 18, JPL Publication 15–10*. Pasadena, CA: Jet Propulsion Laboratory. Retrieved from <http://jpldataeval.jpl.nasa.gov/>
- Cai, Y., Montague, D. C., Mooiweer-Bryan, W., & Deshler, T. (2008). Performance characteristics of the ultra high sensitivity aerosol spectrometer for particles between 55 and 800 nm: Laboratory and field studies. *Journal of Aerosol Science*, 39(9), 759–769. <https://doi.org/10.1016/j.jaerosci.2008.04.007>
- Carpenter, L. J., & Liss, P. S. (2000). On temperate sources of bromoform and other reactive organic bromine gases. *Journal of Geophysical Research*, 105(D16), 20,539–20,547. <https://doi.org/10.1029/2000JD900242>
- Carpenter, L. J., Reimann, S., Burkholder, J. B., Clerbaux, C., Hall, B. D., Hossaini, R., et al. (2014). Ozone-depleting substances (ODSs) and other gases of interest to the Montreal Protocol, Chap. 1. In *Scientific Assessment of Ozone Depletion: 2014, Global Ozone Research and Monitoring Project—Report No. 55* (pp. 1.1–1.101). Geneva, Switzerland: World Meteorological Organization.
- Chen, D., Huey, L. G., Tanner, D. J., Salawitch, R. J., Anderson, D. C., Wales, P. A., et al. (2016). Airborne measurements of BrO and the sum of HOBr and Br<sub>2</sub> over the Tropical West Pacific from 1 to 15 km during the CONvective TRansport of Active Species in the Tropics (CONTRAST) experiment. *Journal of Geophysical Research: Atmospheres*, 121, 12,560–12,578. <https://doi.org/10.1002/2016JD025561>
- Chipperfield, M. P. (2006). New version of the TOMCAT/SILMCAT off-line chemical transport model: Intercomparison of stratospheric tracer experiments. *Quarterly Journal of the Royal Meteorological Society*, 132(617), 1179–1203. <https://doi.org/10.1256/qj.0551>
- Choi, S., Wang, Y., Salawitch, R. J., Canty, T., Joiner, J., Zeng, T., et al. (2012). Analysis of satellite-derived Arctic tropospheric BrO columns in conjunction with aircraft measurements during ARCTAS and ARCPAC. *Atmospheric Chemistry and Physics*, 12(3), 1255–1285. <https://doi.org/10.5194/acp-12-1255-2012>
- Crosson, E. R. (2008). A cavity ring-down analyzer for measuring atmospheric levels of methane, carbon dioxide, and water vapor. *Applied Physics B*, 92(3), 403–408. <https://doi.org/10.1007/s00340-008-3135-y>
- Dee, D. P., Uppala, S. M., Simmons, A. J., Berrisford, P., Poli, P., Kobayashi, S., et al. (2011). The ERA-Interim reanalysis: Configuration and performance of the data assimilation system. *Quarterly Journal of the Royal Meteorological Society*, 137(656), 553–597. <https://doi.org/10.1002/qj.828>
- Deushi, M., & Shibata, K. (2011). Development of a Meteorological Research Institute chemistry-climate model version 2 for the study of tropospheric and stratospheric chemistry. *Papers in Meteorology and Geophysics*, 62, 1–46. <https://doi.org/10.2467/mripapers.62.1>
- Dix, B., Koenig, T. K., & Volkamer, R. (2016). Parameterization retrieval of trace gas volume mixing ratios from Airborne MAX-DOAS. *Atmospheric Measurement Techniques*, 9(11), 5655–5675. <https://doi.org/10.5194/amt-9-5655-2016>
- Dorf, M., Butler, J. H., Butz, A., Camy-Peyret, C., Chipperfield, M. P., Kritten, L., et al. (2006). Long-term observations of stratospheric bromine reveal slow down in growth. *Geophysical Research Letters*, 33, L24803. <https://doi.org/10.1029/2006GL027714>
- Dorf, M., Butz, A., Camy-Peyret, C., Chipperfield, M. P., Kritten, L., & Pfeilsticker, K. (2008). Bromine in the tropical troposphere and stratosphere as derived from balloon-borne BrO observations. *Atmospheric Chemistry and Physics*, 8(23), 7265–7271. <https://doi.org/10.5194/acp-8-7265-2008>
- Dougllass, A., Fioletov, V., Godin-Beekmann, S., Müller, R., Stolarski, R. S., & Webb, A. (2011). Stratospheric ozone and surface ultraviolet radiation, Chap. 2. In *Scientific Assessment of Ozone Depletion: 2010, Global Ozone Research and Monitoring Project—Report No. 52* (pp. 2.1–2.76). Geneva, Switzerland: World Meteorological Organization.
- Dvortsov, V. L., Geller, M. A., Solomon, S., Schauffler, S. M., Atlas, E. L., & Blake, D. R. (1999). Rethinking reactive halogen budgets in the midlatitude lower stratosphere. *Geophysical Research Letters*, 26(12), 1699–1702. <https://doi.org/10.1029/1999GL000309>
- Engel, A., Strunk, M., Müller, M., Haase, H.-P., Poss, C., Levin, I., & Schmidt, U. (2002). Temporal development of total chlorine in the high-latitude stratosphere based on reference distributions of mean age derived from CO<sub>2</sub> and SF<sub>6</sub>. *Journal of Geophysical Research*, 107(12), 4136. <https://doi.org/10.1029/2001JD000584>
- Eyring, V., Lamarque, J.-F., Hess, P., Arfeuille, F., Bowman, K., Chipperfield, M. P., et al. (2013). Overview of IGAC/SPARC Chemistry-Climote Model Initiative (CCMI) community simulations in support of upcoming ozone and climate assessments. *SPARC Newsletter*, 40, 48–66. Retrieved from [http://www.sparc-climate.org/fileadmin/customer/6\\_Publications/Newsletter\\_PDF/40\\_SPARCnewsletter\\_Jan2013\\_web.pdf](http://www.sparc-climate.org/fileadmin/customer/6_Publications/Newsletter_PDF/40_SPARCnewsletter_Jan2013_web.pdf)
- Falk, S., Sinnhuber, B.-M., Krysztofaki, G., Jöckel, P., Graf, P., & Lennartz, S. T. (2017). Brominated VLSL and their influence on ozone under a changing climate. *Atmospheric Chemistry and Physics*, 17(18), 11,313–11,329. <https://doi.org/10.5194/acp-17-11313-2017>
- Feng, W., Chipperfield, M. P., Dorf, M., Pfeilsticker, K., & Ricaud, P. (2007). Mid-latitude ozone changes: Studies with a 3-D CTM forced by ERA-40 analyses. *Atmospheric Chemistry and Physics*, 7(9), 2357–2369. <https://doi.org/10.5194/acp-7-2357-2007>

- Fernandez, R. P., Kinnison, D. E., Lamarque, J.-F., Tilmes, S., & Saiz-Lopez, A. (2017). Impact of biogenic very short-lived bromine on the Antarctic ozone hole during the 21st century. *Atmospheric Chemistry and Physics*, *17*(3), 1673–1688. <https://doi.org/10.5194/acp-17-1673-2017>
- Fernandez, R. P., Salawitch, R. J., Kinnison, D. E., Lamarque, J. F., & Saiz-Lopez, A. (2014). Bromine partitioning in the tropical tropopause layer: Implications for stratospheric injection. *Atmospheric Chemistry and Physics*, *14*(24), 13,391–13,410. <https://doi.org/10.5194/acp-14-13391-2014>
- Fiehn, A., Quack, B., Stemmler, I., Ziska, F., & Krüger, K. (2018). Importance of seasonally resolved oceanic emissions for bromoform delivery from the tropical Indian Ocean and West Pacific to the stratosphere. *Atmospheric Chemistry and Physics Discussions*, 1–37. <https://doi.org/10.5194/acp-2018-92>
- Garcia, R. R., Smith, A. K., Kinnison, D. E., de la Cámara, Á., & Murphy, D. J. (2017). Modification of the gravity wave parameterization in the Whole Atmosphere Community Climate Model: motivation and results. *Journal of the Atmospheric Sciences*, *74*(1), 275–291. <https://doi.org/10.1175/JAS-D-16-0104.1>
- Gerbig, C., Schmitgen, S., Kley, D., Volz-Thomas, A., Dewey, K., & Haaks, D. (1999). An improved fast-response vacuum-UV resonance fluorescence CO instrument. *Journal of Geophysical Research*, *104*(D1), 1699–1704. <https://doi.org/10.1029/1998JD100031>
- Gettelman, A., Hoor, P., Pan, L. L., Randel, W. J., Hegglin, M. I., & Birner, T. (2011). The extratropical upper troposphere and lower stratosphere. *Reviews of Geophysics*, *49*, RG3003. <https://doi.org/10.1029/2011RG000355>
- Hall, T. M., & Plumb, R. A. (1994). Age as a diagnostic of stratospheric transport. *Journal of Geophysical Research*, *99*(D1), 1059–1070. <https://doi.org/10.1029/93JD03192>
- Harris, N. R. P., Carpenter, L. J., Lee, J. D., Vaughan, G., Filus, M. T., Jones, R. L., et al. (2017). Coordinated Airborne Studies in the Tropics (CAST). *Bulletin of the American Meteorological Society*, *98*(1), 145–162. <https://doi.org/10.1175/BAMS-D-14-00290.1>
- Harris, N. R. P., Wuebbles, D. J., Daniel, J. S., Hu, J., Kuijpers, L. J. M., Law, K. S., et al. (2014). Scenarios and information for policymakers, Chap. 5. In *Scientific Assessment of Ozone Depletion: 2014, Global Ozone Research and Monitoring Project—Report No. 55* (pp. 5.1–5.58). Geneva, Switzerland: World Meteorological Organization.
- Holton, J. R., Haynes, P. H., McIntyre, M. E., Douglass, A. R., Rood, R. B., & Pfister, L. (1995). Stratosphere-troposphere exchange. *Reviews of Geophysics*, *33*(4), 403–439. <https://doi.org/10.1029/95RG02097>
- Hossaini, R., Chipperfield, M. P., Feng, W., Breider, T. J., Atlas, E., Montzka, S. A., et al. (2012). The contribution of natural and anthropogenic very short-lived species to stratospheric bromine. *Atmospheric Chemistry and Physics*, *12*(1), 371–380. <https://doi.org/10.5194/acp-12-371-2012>
- Hossaini, R., Chipperfield, M. P., Monge-Sanz, B. M., Richards, N. A. D., Atlas, E., & Blake, D. R. (2010). Bromoform and dibromomethane in the tropics: A 3-D model study of chemistry and transport. *Atmospheric Chemistry and Physics*, *10*(2), 719–735. <https://doi.org/10.5194/acp-10-719-2010>
- Hossaini, R., Mantle, H., Chipperfield, M. P., Montzka, S. A., Hamer, P., Ziska, F., et al. (2013). Evaluating global emission inventories of biogenic bromocarbons. *Atmospheric Chemistry and Physics*, *13*(23), 11,819–11,838. <https://doi.org/10.5194/acp-13-11819-2013>
- Hossaini, R., Patra, P. K., Leeson, A. A., Krysztofiak, G., Abraham, N. L., Andrews, S. J., et al. (2016). A multi-model intercomparison of halogenated very short-lived substances (TransCom-VLSL): Linking oceanic emissions and tropospheric transport for a reconciled estimate of the stratospheric source gas injection of bromine. *Atmospheric Chemistry and Physics*, *16*(14), 9163–9187. <https://doi.org/10.5194/acp-16-9163-2016>
- Huey, L. G. (2007). Measurement of trace atmospheric species by chemical ionization mass spectrometry: Speciation of reactive nitrogen and future directions. *Mass Spectrometry Reviews*, *26*(2), 166–184. <https://doi.org/10.1002/mas.20118>
- Jensen, E. J., Pfister, L., Jordan, D. E., Bui, T. V., Ueyama, R., Singh, H. B., et al. (2017). The NASA Airborne Tropical Tropopause Experiment: High-altitude aircraft measurements in the Tropical Western Pacific. *Bulletin of the American Meteorological Society*, *98*(1), 129–143. <https://doi.org/10.1175/BAMS-D-14-00263.1>
- Jöckel, P., Tost, H., Pozzer, A., Kunze, M., Kirner, O., Brenninkmeijer, C. A. M., et al. (2016). Earth System Chemistry integrated Modelling (ESCI-Mo) with the Modular Earth Submodel System (MESSy) version 2.51. *Geoscientific Model Development*, *9*(3), 1153–1200. <https://doi.org/10.5194/gmd-9-1153-2016>
- Kerkweg, A., Jöckel, P., Warwick, N., Gebhardt, S., Brenninkmeijer, C. A. M., & Lelieveld, J. (2008). Consistent simulation of bromine chemistry from the marine boundary layer to the stratosphere—Part 2: Bromocarbons. *Atmospheric Chemistry and Physics*, *8*(19), 5919–5939. <https://doi.org/10.5194/acp-8-5919-2008>
- Klobas, J. E., Wilmouth, D. M., Weisenstein, D. K., Anderson, J. G., & Salawitch, R. J. (2017). Ozone depletion following future volcanic eruptions. *Geophysical Research Letters*, *44*, 7490–7499. <https://doi.org/10.1002/2017GL073972>
- Ko, M. K. W., Poulet, G., Blake, D. R., Boucher, O., Burkholder, J. H., Chin, M., et al. (2003). Very short-lived halogen and sulfur substances, Chap. 2. In *Scientific Assessment of Ozone Depletion: 2002, Global Ozone Research and Monitoring Project—Report No. 47* (pp. 2.1–2.57). Geneva, Switzerland: World Meteorological Organization.
- Ko, M. K. W., Sze, N., Scott, C. J., & Weisenstein, D. K. (1997). On the relation between stratospheric chlorine/bromine loading and short-lived tropospheric source gases. *Journal of Geophysical Research*, *102*(D21), 25,507–25,517. <https://doi.org/10.1029/97JD02431>
- Koenig, T. K., Volkamer, R., Baidar, S., Dix, B., Wang, S., Anderson, D. C., et al. (2017). BrO and inferred Br<sub>y</sub> profiles over the western Pacific: Relevance of inorganic bromine sources and a Br<sub>y</sub> minimum in the aged tropical tropopause layer. *Atmospheric Chemistry and Physics*, *17*(24), 15,245–15,270. <https://doi.org/10.5194/acp-17-15245-2017>
- Kovalenko, L. J., Livesey, N. L., Salawitch, R. J., Camy-Peyret, C., Chipperfield, M. P., Cofield, R. E., et al. (2007). Validation of Aura Microwave Limb Sounder BrO observations in the stratosphere. *Journal of Geophysical Research*, *112*, D24541. <https://doi.org/10.1029/2007JD008817>
- Kreycy, S., Camy-Peyret, C., Chipperfield, M. P., Dorf, M., Feng, W., Hossaini, R., et al. (2013). Atmospheric test of the J(BrONO<sub>2</sub>)/k<sub>BrO+NO<sub>2</sub></sub> ratio: Implications for total stratospheric Br<sub>y</sub> and bromine-mediated ozone loss. *Atmospheric Chemistry and Physics*, *13*(13), 6263–6274. <https://doi.org/10.5194/acp-13-6263-2013>
- Lamarque, J.-F., Emmons, L. K., Hess, P. G., Kinnison, D. E., Tilmes, S., Vitt, F., et al. (2012). CAM-chem: Description and evaluation of interactive atmospheric chemistry in the Community Earth System Model. *Geoscientific Model Development*, *5*(2), 369–411. <https://doi.org/10.5194/gmd-5-369-2012>
- Laube, J. C., Engel, A., Bönisch, H., Möbius, T., Worton, D. R., Sturges, W. T., et al. (2008). Contribution of very short-lived organic substances to stratospheric chlorine and bromine in the tropics—A case study. *Atmospheric Chemistry and Physics*, *8*(23), 7325–7334. <https://doi.org/10.5194/acp-8-7325-2008>
- Le Breton, M., Bannan, T. J., Shallcross, D. E., Khan, M. A., Evans, M. J., Lee, J., et al. (2017). Enhanced ozone loss by active inorganic bromine chemistry in the tropical troposphere. *Atmospheric Environment*, *155*, 21–28. <https://doi.org/10.1016/j.atmosenv.2017.02.003>

- Lennartz, S. T., Krysztofciak, G., Marandino, C. A., Sinnhuber, B. M., Tegtmeier, S., Ziska, F., et al. (2015). Modelling marine emissions and atmospheric distributions of halocarbons and dimethyl sulfide: The influence of prescribed water concentration vs. prescribed emissions. *Atmospheric Chemistry and Physics*, *15*(20), 11,753–11,772. <https://doi.org/10.5194/acp-15-11753-2015>
- Levine, J. G., Braesicke, P., Harris, N. R. P., Savage, N. H., & Pyle, J. A. (2007). Pathways and timescales for troposphere-to-stratosphere transport via the tropical tropopause layer and their relevance for very short lived substances. *Journal of Geophysical Research*, *112*, D04308. <https://doi.org/10.1029/2005JD006940>
- Liang, Q., Atlas, E., Blake, D., Dorf, M., Pfeilsticker, K., & Schauffler, S. (2014). Convective transport of very short lived bromocarbons to the stratosphere. *Atmospheric Chemistry and Physics*, *14*(11), 5781–5792. <https://doi.org/10.5194/acp-14-5781-2014>
- Liang, Q., Stolarski, R. S., Kawa, S. R., Nielsen, J. E., Douglass, A. R., Rodriguez, J. M., et al. (2010). Finding the missing stratospheric Br<sub>y</sub>: A global modeling study of CHBr<sub>3</sub> and CH<sub>2</sub>Br<sub>2</sub>. *Atmospheric Chemistry and Physics*, *10*(5), 2269–2286. <https://doi.org/10.5194/acp-10-2269-2010>
- Liao, J., Sihler, H., Huey, L. G., Neuman, J. A., Tanner, D. J., Friess, U., et al. (2011). A comparison of Arctic BrO measurements by chemical ionization mass spectrometry and long path-differential optical absorption spectroscopy. *Journal of Geophysical Research*, *116*, D00R02. <https://doi.org/10.1029/2010JD014788>
- Long, M. S., Keene, W. C., Easter, R. C., Sander, R., Liu, X., Kerkweg, A., & Erickson, D. (2014). Sensitivity of tropospheric chemical composition to halogen-radical chemistry using a fully coupled size-resolved multiphase chemistry-global climate system: Halogen distributions, aerosol composition, and sensitivity of climate-relevant gases. *Atmospheric Chemistry and Physics*, *14*(7), 3397–3425. <https://doi.org/10.5194/acp-14-3397-2014>
- Marsh, D. R., Mills, M. J., Kinnison, D. E., Lamarque, J. F., Calvo, N., & Polvani, L. M. (2013). Climate change from 1850 to 2005 simulated in CESM1(WACCM). *Journal of Climate*, *26*(19), 7372–7391. <https://doi.org/10.1175/JCLI-D-12-00558.1>
- McLinden, C. A., Haley, C. S., Lloyd, N. D., Hendrick, F., Rozanov, A., Sinnhuber, B. M., et al. (2010). Odin/OSIRIS observations of stratospheric BrO: Retrieval methodology, climatology, and inferred Br<sub>y</sub>. *Journal of Geophysical Research*, *115*, D15308. <https://doi.org/10.1029/2009JD012488>
- Michou, M., Saint-Martin, D., Teyssède, H., Alias, A., Karcher, F., Ollivé, D., et al. (2011). A new version of the CNRM Chemistry-Climate Model, CNRM-CCM: Description and improvements from the CCMVal-2 simulations. *Geoscientific Model Development*, *4*(4), 873–900. <https://doi.org/10.5194/gmd-4-873-2011>
- Mohd Nadzir, M. S., Phang, S. M., Abas, M. R., Abdul Rahman, N., Abu Samah, A., Sturges, W. T., et al. (2014). Bromocarbons in the tropical coastal and open ocean atmosphere during the 2009 Prime Expedition Scientific Cruise (PESC-09). *Atmospheric Chemistry and Physics*, *14*(15), 8137–8148. <https://doi.org/10.5194/acp-14-8137-2014>
- Molod, A., Takacs, L., Suarez, M., Bacmeister, J., Song, I., & Eichmann, A. (2012). The GEOS-5 atmospheric general circulation model: Mean climate and development from MERRA to Fortuna. Technical Report Series on Global Modeling and Data Assimilation, 27.
- Montzka, S. A., Reimann, S., Engel, A., Krüger, K., Sturges, W. T., & O'Doherty, S. (2011). Ozone-depleting substances (ODSs) and related chemicals, Chap. 1. In *Scientific Assessment of Ozone Depletion: 2010. Global Ozone Research and Monitoring Project—Report No. 52* (52nd ed., pp. 1.1–1.108). Geneva, Switzerland: World Meteorological Organization.
- Morgenstern, O., Braesicke, P., O'Connor, F. M., Bushell, A. C., Johnson, C. E., Osprey, S. M., & Pyle, J. A. (2009). Evaluation of the new UKCA climate-composition model—Part 1: The stratosphere. *Geoscientific Model Development*, *2*(1), 43–57. <https://doi.org/10.5194/gmd-2-43-2009>
- Morgenstern, O., Hegglin, M. I., Rozanov, E., O'Connor, F. M., Abraham, N. L., Akiyoshi, H., et al. (2017). Review of the global models used within phase 1 of the Chemistry–Climate Model Initiative (CCMI). *Geoscientific Model Development*, *10*(2), 639–671. <https://doi.org/10.5194/gmd-10-639-2017>
- Morgenstern, O., Stone, K. A., Schofield, R., Akiyoshi, H., Yamashita, Y., Kinnison, D. E., et al. (2018). Ozone sensitivity to varying greenhouse gases and ozone-depleting substances in CCMI-1 simulations. *Atmospheric Chemistry and Physics*, *18*(2), 1091–1114. <https://doi.org/10.5194/acp-18-1091-2018>
- Navarro, M. A., Atlas, E. L., Saiz-Lopez, A., Rodriguez-Lloveras, X., Kinnison, D. E., Lamarque, J., et al. (2015). Airborne measurements of organic bromine compounds in the Pacific tropical tropopause layer. *Proceedings of the National Academy of Sciences of the United States of America*, *112*(45), 13,789–13,793. <https://doi.org/10.1073/pnas.1511463112>
- Navarro, M. A., Saiz-Lopez, A., Cuevas, C. A., Fernandez, R. P., Atlas, E., Rodriguez-Lloveras, X., et al. (2017). Modeling the inorganic bromine partitioning in the tropical tropopause layer over the eastern and western Pacific Ocean. *Atmospheric Chemistry and Physics*, *17*(16), 9917–9930. <https://doi.org/10.5194/acp-17-9917-2017>
- Nicely, J. M., Anderson, D. C., Canty, T. P., Salawitch, R. J., Wolfe, G. M., Apel, E. C., et al. (2016). An observationally constrained evaluation of the oxidative capacity in the tropical western Pacific troposphere. *Journal of Geophysical Research: Atmospheres*, *121*, 7461–7488. <https://doi.org/10.1002/2016JD025067>
- Oman, L. D., Douglass, A. R., Salawitch, R. J., Canty, T. P., Ziemke, J. R., & Manyin, M. (2016). The effect of representing bromine from VLSL on the simulation and evolution of Antarctic ozone. *Geophysical Research Letters*, *43*, 9869–9876. <https://doi.org/10.1002/2016GL070471>
- Oman, L. D., Douglass, A. R., Ziemke, J. R., Rodriguez, J. M., Waugh, D. W., & Nielsen, J. E. (2013). The ozone response to ENSO in Aura satellite measurements and a chemistry-climate simulation. *Journal of Geophysical Research: Atmospheres*, *118*, 965–976. <https://doi.org/10.1029/2012JD018546>
- Ordóñez, C., Lamarque, J. F., Tilmes, S., Kinnison, D. E., Atlas, E. L., Blake, D. R., et al. (2012). Bromine and iodine chemistry in a global chemistry-climate model: Description and evaluation of very short-lived oceanic sources. *Atmospheric Chemistry and Physics*, *12*(3), 1423–1447. <https://doi.org/10.5194/acp-12-1423-2012>
- Pan, L. L., Atlas, E. L., Salawitch, R. J., Honomichl, S. B., Bresch, J. F., Randel, W. J., et al. (2017). The Convective Transport of Active Species in the Tropics (CONTRAST) Experiment. *Bulletin of the American Meteorological Society*, *98*(1), 106–128. <https://doi.org/10.1175/BAMS-D-14-00272.1>
- Pan, L. L., Bowman, K. P., Shapiro, M., Randel, W. J., Gao, R. S., Campos, T., et al. (2007). Chemical behavior of the tropopause observed during the Stratosphere-Troposphere Analyses of Regional Transport experiment. *Journal of Geophysical Research*, *112*, D18110. <https://doi.org/10.1029/2007JD008645>
- Pan, L. L., Randel, W. J., Gary, B. L., Mahoney, M. J., & Hints, E. J. (2004). Definitions and sharpness of the extratropical tropopause: A trace gas perspective. *Journal of Geophysical Research*, *109*, D23103. <https://doi.org/10.1029/2004JD004982>
- Parrella, J. P., Chance, K., Salawitch, R. J., Canty, T., Dorf, M., & Pfeilsticker, K. (2013). New retrieval of BrO from SCIAMACHY limb: An estimate of the stratospheric bromine loading during April 2008. *Atmospheric Measurement Techniques*, *6*(10), 2549–2561. <https://doi.org/10.5194/amt-6-2549-2013>
- Pfeilsticker, K., Sturges, W. T., Bösch, H., Camy-Peyret, C., Chipperfield, M. P., Engel, A., et al. (2000). Lower stratospheric organic and inorganic bromine budget for the Arctic winter 1998/99. *Geophysical Research Letters*, *27*(20), 3305–3308. <https://doi.org/10.1029/2000GL011650>

- Pitari, G., Aquila, V., Kravitz, B., Robock, A., Watanabe, S., Cionni, I., et al. (2014). Stratospheric ozone response to sulfate geoengineering: Results from the Geoengineering Model Intercomparison Project (GeoMIP). *Journal of Geophysical Research: Atmospheres*, *119*, 2629–2653. <https://doi.org/10.1002/2013JD020566>
- Plumb, R. A., & Ko, M. K. W. (1992). Interrelationships between mixing ratios of long-lived stratospheric constituents. *Journal of Geophysical Research*, *97*(D9), 10,145–10,156. <https://doi.org/10.1029/92JD00450>
- Prinn, R. G., Weiss, R. F., Fraser, P. J., Simmonds, P. G., Cunnold, D. M., Aleya, F. N., et al. (2000). A history of chemically and radiatively important gases in air deduced from ALE/GAGE/AGAGE. *Journal of Geophysical Research*, *105*(D14), 17,751–17,792. <https://doi.org/10.1029/2000JD900141>
- Pyle, J. A., Ashfold, M. J., Harris, N. R. P., Robinson, A. D., Warwick, N. J., Carver, G. D., et al. (2011). Bromoform in the tropical boundary layer of the Maritime Continent during OP3. *Atmospheric Chemistry and Physics*, *11*(2), 529–542. <https://doi.org/10.5194/acp-11-529-2011>
- Quack, B., & Wallace, D. W. R. (2003). Air-sea flux of bromoform: Controls, rates, and implications. *Global Biogeochemical Cycles*, *17*(1), 1023. <https://doi.org/10.1029/2002GB001890>
- Revell, L. E., Stenke, A., Luo, B., Kremser, S., Rozanov, E., Sukhodolov, T., & Peter, T. (2017). Impacts of Mt Pinatubo volcanic aerosol on the tropical stratosphere in chemistry-climate model simulations using CCM1 and CMIP6 stratospheric aerosol data. *Atmospheric Chemistry and Physics*, *17*(21), 13,139–13,150. <https://doi.org/10.5194/acp-17-13139-2017>
- Rex, M., Wohltmann, I., Ridder, T., Lehmann, R., Rosenlof, K., Wennberg, P., et al. (2014). A tropical West Pacific OH minimum and implications for stratospheric composition. *Atmospheric Chemistry and Physics*, *14*(9), 4827–4841. <https://doi.org/10.5194/acp-14-4827-2014>
- Ridley, B. A., & Grahek, F. E. (1990). A small, low flow, high sensitivity reaction vessel for NO chemiluminescence detectors. *Journal of Atmospheric and Oceanic Technology*, *7*(2), 307–311. [https://doi.org/10.1175/1520-0426\(1990\)007%3C0307:ASLFHS%3E2.0.CO;2](https://doi.org/10.1175/1520-0426(1990)007%3C0307:ASLFHS%3E2.0.CO;2)
- Robinson, A. D., Harris, N. R. P., Ashfold, M. J., Gostlow, B., Warwick, N. J., O'Brien, L. M., et al. (2014). Long-term halocarbon observations from a coastal and an inland site in Sabah, Malaysian Borneo. *Atmospheric Chemistry and Physics*, *14*(16), 8369–8388. <https://doi.org/10.5194/acp-14-8369-2014>
- Saiz-Lopez, A., Fernandez, R. P., Ordóñez, C., Kinnison, D. E., Martín, J. C. G., Lamarque, J. F., & Tilmes, S. (2014). Iodine chemistry in the troposphere and its effect on ozone. *Atmospheric Chemistry and Physics*, *14*(23), 13,119–13,143. <https://doi.org/10.5194/acp-14-13119-2014>
- Sala, S., Bönisch, H., Keber, T., Oram, D. E., Mills, G., & Engel, A. (2014). Deriving an atmospheric budget of total organic bromine using airborne in situ measurements from the western Pacific area during SHIVA. *Atmospheric Chemistry and Physics*, *14*(13), 6903–6923. <https://doi.org/10.5194/acp-14-6903-2014>
- Salawitch, R. J., Canty, T., Kurosu, T., Chance, K., Liang, Q., Da Silva, A., et al. (2010). A new interpretation of total column BrO during Arctic spring. *Geophysical Research Letters*, *37*, L21805. <https://doi.org/10.1029/2010GL043798>
- Salawitch, R. J., Weisenstein, D. K., Kovalenko, L. J., Sioris, C. E., Wennberg, P. O., Chance, K., et al. (2005). Sensitivity of ozone to bromine in the lower stratosphere. *Geophysical Research Letters*, *32*, L05811. <https://doi.org/10.1029/2004GL021504>
- Schauffler, S. M., Atlas, E. L., Blake, D. R., Flocke, F., Lueb, R. A., Lee-Taylor, J. M., et al. (1999). Distributions of brominated organic compounds in the troposphere and lower stratosphere. *Journal of Geophysical Research*, *104*(D17), 21,513–21,535. <https://doi.org/10.1029/1999JD900197>
- Schauffler, S. M., Atlas, E. L., Donnelly, S. G., Andrews, A., Montzka, S. A., Elkins, J. W., et al. (2003). Chlorine budget and partitioning during the Stratospheric Aerosol and Gas Experiment (SAGE) III Ozone Loss and Validation Experiment (SOLVE). *Journal of Geophysical Research*, *108*(D5), 4173. <https://doi.org/10.1029/2001JD002040>
- Schmidt, J. A., Jacob, D. J., Horowitz, H. M., Hu, L., Sherwen, T., Evans, M. J., et al. (2016). Modeling the observed tropospheric BrO background: Importance of multiphase chemistry and implications for ozone, OH, and mercury. *Journal of Geophysical Research: Atmospheres*, *121*, 11,819–11,835. <https://doi.org/10.1002/2015JD024229>
- Schofield, R., Fueglistaler, S., Wohltmann, I., & Rex, M. (2011). Sensitivity of stratospheric Br<sub>2</sub> to uncertainties in very short lived substance emissions and atmospheric transport. *Atmospheric Chemistry and Physics*, *11*(4), 1379–1392. <https://doi.org/10.5194/acp-11-1379-2011>
- Schofield, R., Kreher, K., Conner, B. J., Johnston, P. V., Thomas, A., Shooter, D., et al. (2004). Retrieved tropospheric and stratospheric BrO columns over lauder, New Zealand. *Journal of Geophysical Research*, *109*, D14304. <https://doi.org/10.1029/2003JD004463>
- Scinocca, J. F., McFarlane, N. A., Lazare, M., Li, J., & Plummer, D. (2008). Technical note: The CCCma third generation AGCM and its extension into the middle atmosphere. *Atmospheric Chemistry and Physics*, *8*(23), 7055–7074. <https://doi.org/10.5194/acp-8-7055-2008>
- Shetter, R. E., & Müller, M. (1999). Photolysis frequency measurements using actinic flux spectroradiometry during the PEM-Tropics mission: Instrumentation description and some results. *Journal of Geophysical Research*, *104*(D5), 5647–5661. <https://doi.org/10.1029/98JD01381>
- Sinnhuber, B.-M., & Folkins, I. (2006). Estimating the contribution of bromoform to stratospheric bromine and its relation to dehydration in the tropical tropopause layer. *Atmospheric Chemistry and Physics*, *6*(12), 4755–4761. <https://doi.org/10.5194/acp-6-4755-2006>
- Sinnhuber, B. M., & Meul, S. (2015). Simulating the impact of emissions of brominated very short lived substances on past stratospheric ozone trends. *Geophysical Research Letters*, *42*, 2449–2456. <https://doi.org/10.1002/2014GL062975>
- Sioris, C. E., Kovalenko, L. J., McLinden, C. A., Salawitch, R. J., Van Roozendaal, M., Goutail, F., et al. (2006). Latitudinal and vertical distribution of bromine monoxide in the lower stratosphere from Scanning Imaging Absorption Spectrometer for Atmospheric Chartography limb scattering measurements. *Journal of Geophysical Research*, *111*, D14301. <https://doi.org/10.1029/2005JD006479>
- Solomon, S., Kinnison, D., Bandoro, J., & Garcia, R. (2015). Simulation of polar ozone depletion: An update. *Journal of Geophysical Research: Atmospheres*, *120*, 7958–7974. <https://doi.org/10.1002/2015JD023365>
- SPARC (2013). M. Ko, P. Newman, S. Reimann, & S. Strahan (Eds.), *SPARC report on lifetimes of stratospheric ozone-depleting substances, their replacements, and related species*. SPARC Report No. 6, WCRP-15/2013. Oberpfaffenhofen, Germany: SPARC Office. Retrieved from <http://www.sparc-climate.org/publications/sparc-reports/>
- Stachnik, R. A., Millán, L., Jarnot, R., Monroe, R., McLinden, C., Kühl, S., et al. (2013). Stratospheric BrO abundance measured by a balloon-borne submillimeterwave radiometer. *Atmospheric Chemistry and Physics*, *13*(6), 3307–3319. <https://doi.org/10.5194/acp-13-3307-2013>
- Stenke, A., Schraner, M., Rozanov, E., Egorova, T., Luo, B., & Peter, T. (2013). The SOCOL version 3.0 chemistry-climate model: Description, evaluation, and implications from an advanced transport algorithm. *Geoscientific Model Development*, *6*(5), 1407–1427. <https://doi.org/10.5194/gmd-6-1407-2013>
- Stone, K. A., Morgenstern, O., Karoly, D. J., Klekociuk, A. R., French, W. J., Abraham, N. L., & Schofield, R. (2016). Evaluation of the ACCESS-Chemistry-climate model for the Southern Hemisphere. *Atmospheric Chemistry and Physics*, *16*(4), 2401–2415. <https://doi.org/10.5194/acp-16-2401-2016>
- Stutz, J., Werner, B., Spolaoar, M., Scalone, L., Festa, J., Tsai, C., et al. (2017). A new differential optical absorption spectroscopy instrument to study atmospheric chemistry from a high-altitude unmanned aircraft. *Atmospheric Measurement Techniques*, *10*(3), 1017–1042. <https://doi.org/10.5194/amt-10-1017-2017>
- Tegtmeier, S., Krüger, K., Quack, B., Atlas, E. L., Pisso, I., Stohl, A., & Yang, X. (2012). Emission and transport of bromocarbons: From the West Pacific ocean into the stratosphere. *Atmospheric Chemistry and Physics*, *12*(22), 10,633–10,648. <https://doi.org/10.5194/acp-12-10633-2012>

- Theys, N., Van Roozendael, M., Hendrick, F., Fayt, C., Hermans, C., Baray, J.-L., et al. (2007). Retrieval of stratospheric and tropospheric BrO columns from multi-axis DOAS measurements at Reunion Island (21°S, 56°E). *Atmospheric Chemistry and Physics*, 7(18), 4733–4749. <https://doi.org/10.5194/acp-7-4733-2007>
- Theys, N., Van Roozendael, M., Hendrick, F., Yang, X., De Smedt, I., Richter, A., et al. (2011). Global observations of tropospheric BrO columns using GOME-2 satellite data. *Atmospheric Chemistry and Physics*, 11(4), 1791–1811. <https://doi.org/10.5194/acp-11-1791-2011>
- Tian, W., & Chipperfield, M. P. (2005). A new coupled chemistry–climate model for the stratosphere: The importance of coupling for future O<sub>3</sub>-climate predictions. *Quarterly Journal of the Royal Meteorological Society*, 131(605), 281–303. <https://doi.org/10.1256/qj.04.05>
- Tilmes, S., Kinnison, D. E., Garcia, R. R., Salawitch, R., Canty, T., Lee-Taylor, J., et al. (2012). Impact of very short-lived halogens on stratospheric ozone abundance and UV radiation in a geo-engineered atmosphere. *Atmospheric Chemistry and Physics*, 12(22), 10,945–10,955. <https://doi.org/10.5194/acp-12-10945-2012>
- Tilmes, S., Lamarque, J.-F., Emmons, L. K., Kinnison, D. E., Ma, P.-L., Liu, X., et al. (2015). Description and evaluation of tropospheric chemistry and aerosols in the Community Earth System Model (CESM1.2). *Geoscientific Model Development*, 8(5), 1395–1426. <https://doi.org/10.5194/gmd-8-1395-2015>
- Tilmes, S., Lamarque, J. F., Emmons, L. K., Kinnison, D. E., Marsh, D., Garcia, R. R., et al. (2016). Representation of the Community Earth System Model (CESM1) CAM4-chem within the Chemistry-Climate Model Initiative (CCMI). *Geoscientific Model Development*, 9(5), 1853–1890. <https://doi.org/10.5194/gmd-9-1853-2016>
- Tilmes, S., Müller, R., & Salawitch, R. (2008). The sensitivity of polar ozone depletion to proposed geoengineering schemes. *Science*, 320(5880), 1201–1204. <https://doi.org/10.1126/science.1153966>
- Tokarczyk, R., & Moore, R. M. (1994). Production of volatile organohalogen by phytoplankton cultures. *Geophysical Research Letters*, 21(4), 285–288. <https://doi.org/10.1029/94GL00009>
- Volz, A., Sanchez-Gomez, E., Salas y Méria, D., Decharme, B., Cassou, C., Sénéci, S., et al. (2012). The CNRM-CM5.1 global climate model: Description and basic evaluation. *Climate Dynamics*, 40(9–10), 2091–2121. <https://doi.org/10.1007/s00382-011-1259-y>
- Volk, C. M., Elkins, J. W., Fahey, D. W., Salawitch, R. J., Dutton, G. S., Gilligan, J. M., et al. (1996). Quantifying transport between the tropical and mid-latitude lower stratosphere. *Science*, 272(5269), 1763–1768. <https://doi.org/10.1126/science.272.5269.1763>
- Volkamer, R., Baidar, S., Campos, T. L., Coburn, S., DiGangi, J. P., Dix, B., et al. (2015). Aircraft measurements of BrO, IO, glyoxal, NO<sub>2</sub>, H<sub>2</sub>O, O<sub>2</sub>–O<sub>2</sub> and aerosol extinction profiles in the tropics: Comparison with aircraft–/ship-based in situ and lidar measurements. *Atmospheric Measurement Techniques*, 8(5), 2121–2148. <https://doi.org/10.5194/amt-8-2121-2015>
- Wamsley, P. R., Elkins, J. W., Fahey, D. W., Dutton, G. S., Volk, C. M., Myers, R. C., et al. (1998). Distribution of halon-1211 in the upper troposphere and lower stratosphere and the 1994 total bromine budget. *Journal of Geophysical Research*, 103(D1), 1513–1526. <https://doi.org/10.1029/97JD02466>
- Wang, S., Schmidt, J. A., Baidar, S., Coburn, S., Dix, B., Koenig, T. K., et al. (2015). Active and widespread halogen chemistry in the tropical and subtropical free troposphere. *Proceedings of the National Academy of Sciences of the United States of America*, 112(30), 9281–9286. <https://doi.org/10.1073/pnas.1505142112>
- Warwick, N. J., Pyle, J. A., Carver, G. D., Yang, X., Savage, N. H., O'Connor, F. M., & Cox, R. A. (2006). Global modeling of biogenic bromocarbons. *Journal of Geophysical Research*, 111, D24305. <https://doi.org/10.1029/2006JD007264>
- Werner, B., Stutz, J., Spolaor, M., Scalone, L., Raecke, R., Festa, J., et al. (2017). Probing the subtropical lowermost stratosphere and the tropical upper troposphere and tropopause layer for inorganic bromine. *Atmospheric Chemistry and Physics*, 17(2), 1161–1186. <https://doi.org/10.5194/acp-17-1161-2017>
- Wisher, A., Oram, D. E., Laube, J. C., Mills, G. P., van Velthoven, P., Zahn, A., & Brenninkmeijer, C. A. M. (2014). Very short-lived bromomethanes measured by the CARIBIC observatory over the North Atlantic, Africa and Southeast Asia during 2009–2013. *Atmospheric Chemistry and Physics*, 14(7), 3557–3570. <https://doi.org/10.5194/acp-14-3557-2014>
- Wofsy, S. C., McElroy, M. B., & Yung, Y. L. (1975). The chemistry of atmospheric bromine. *Geophysical Research Letters*, 2(6), 215–218. <https://doi.org/10.1029/GL002i006p00215>
- World Meteorological Organization (1957). *Meteorology—A three-dimensional science: Second session of the Commission for Aerology*. Geneva, Switzerland: WMO Bull.
- Yang, X., Cox, R. A., Warwick, N. J., Pyle, J. A., Carver, G. D., O'Connor, F. M., & Savage, N. H. (2005). Tropospheric bromine chemistry and its impacts on ozone: A model study. *Journal of Geophysical Research*, 110, D23311. <https://doi.org/10.1029/2005JD006244>
- Yukimoto, S., Adachi, Y., Hosaka, M., Sakami, T., Yoshimura, H., Hirabara, M., et al. (2012). A new global climate model of the Meteorological Research Institute: MRI-CGCM3: Model description and basic performance. *Journal of the Meteorological Society of Japan*, 90A, 23–64. <https://doi.org/10.2151/jmsj.2012-A02>
- Ziska, F., Quack, B., Abrahamsson, K., Archer, S. D., Atlas, E., Bell, T., et al. (2013). Global sea-to-air flux climatology for bromoform, dibromo-methane and methyl iodide. *Atmospheric Chemistry and Physics*, 13(17), 8915–8934. <https://doi.org/10.5194/acp-13-8915-2013>
- Zondlo, M. A., Paige, M. E., Massick, S. M., & Silver, J. A. (2010). Vertical cavity laser hygrometer for the National Science Foundation Gulfstream-V aircraft. *Journal of Geophysical Research*, 115, D20309. <https://doi.org/10.1029/2010JD014445>